

This is a repository copy of Flexural design of cold-formed steel built-up sections failing by local buckling: development of generalised direct strength method.

White Rose Research Online URL for this paper: <a href="https://eprints.whiterose.ac.uk/id/eprint/233287/">https://eprints.whiterose.ac.uk/id/eprint/233287/</a>

Version: Published Version

### Article:

Maizi, S.-E., Hadidane, Y. and Dar, M.A. orcid.org/0000-0003-2782-9225 (2024) Flexural design of cold-formed steel built-up sections failing by local buckling: development of generalised direct strength method. Engineering Structures, 308. 117967. ISSN: 0141-0296

https://doi.org/10.1016/j.engstruct.2024.117967

### Reuse

This article is distributed under the terms of the Creative Commons Attribution (CC BY) licence. This licence allows you to distribute, remix, tweak, and build upon the work, even commercially, as long as you credit the authors for the original work. More information and the full terms of the licence here: https://creativecommons.org/licenses/

### Takedown

If you consider content in White Rose Research Online to be in breach of UK law, please notify us by emailing eprints@whiterose.ac.uk including the URL of the record and the reason for the withdrawal request.

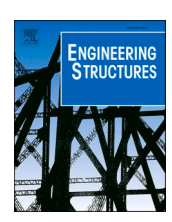


ELSEVIER

Contents lists available at ScienceDirect

# **Engineering Structures**

journal homepage: www.elsevier.com/locate/engstruct





# Flexural design of cold-formed steel built-up sections failing by local buckling: Development of generalised direct strength method

Salah-Eddine Maizi<sup>a</sup>, Yazid Hadidane<sup>a</sup>, Mohammad Adil Dar<sup>b,\*</sup>

- a Laboratory of Civil Engineering (LGC), Department of Civil Engineering, University of Badji Mokhtar, P.O. Box 12, 23000 Annaba, Algeria
- b Department of Civil and Structural Engineering, Faculty of Engineering, University of Sheffield, Sheffield S1 3JD, UK

#### ARTICLE INFO

Keywords:
Beams
Built-up sections
Cold-formed steel
Direct Strength Method
Local buckling
Screw spacing

#### ABSTRACT

This research paper presents a new flexural design approach for cold-formed steel (CFS) built-up sections failing in local buckling, developed following an extensive numerical investigation involving two novel closed built-up sections. At first, a finite element (FE) model using the widely adopted ABAQUS software was constructed and carefully validated against pertinent experimental data available in the literature. A comprehensive validation process which included comparing flexural strengths, deformed shapes, moment-curvature, and momentdisplacement curves was performed. Afterwards, the validated FE model was extended to a numerical parametric investigation comprising of 108 simulations involving both three-point and four-point bending cases. Key parameters, including cross-sectional shapes, slenderness, and screw spacing, were varied primarily to facilitate the formulation of the novel design method. The outcomes of this investigation revealed that the current direct strength method (DSM) available in the North American Specifications (NAS) underestimated the bending strength, particularly for the ultra-thin sections. Considering this observation which is consistent with the findings of past research on similar cross-sections, a Generalised Direct Strength Method (DSM-G) was developed by introducing a new mathematical model, which differs from the traditional slenderness limit equations, instead relying on a conservativeness degree-based approach used for modifying the original DSM equations. The DSM-G method demonstrated a better accuracy in predicting the flexural strengths of different built-up sections (including the ones investigated by other researchers), all failing by local buckling. Moreover, the reliability of DSM-G equations was assessed, satisfying the prescribed threshold index limit suggested in NAS. A comprehensive set of guidelines, along with a design example for implementing the DSM-G method, has been presented to facilitate practical application.

## 1. Introduction

In recent years, the construction industry has witnessed a significant surge in adopting cold-formed thin metal sheets in building construction. This trend is driven by the versatility offered by the cold-forming process, which allows for manufacturing a wide range of shapes and sizes. Due to their lightweight characteristics and ease of transportation, these profiles have emerged as a viable alternative to traditional hotrolled steel members, especially for mid-rise and low-rise structures. However, using thinner steel sections under compression loads poses a significant challenge of being susceptible to buckling stability failures, such as local, global, and distortional buckling. One way to enhance the strength of cold-formed steel (CFS) members under increased loading demands involves adopting built-up back-to-back I-sections formed by

overlapping the webs of two channel sections [1,2]. Nevertheless, the range of built-up shapes available is limited to conventional I-sections with varying stiffener configurations. Moreover, symmetrical closed sections have proven effective in improving torsional buckling rigidity, a feature I-sections lack due to their free flanges [3,4]. This limitation has been addressed by adopting built-up face-to-face sections, resulting in closed sectional profiles [5]. These sections offer a diverse range of shapes by incorporating intermittent stiffeners in both the web and flanges, effectively preventing torsional buckling in extended members and laterally unrestrained spans.

Previous research on built-up sections has focused on exploring and optimising intermittent stiffeners and sectional configurations, which are critical for enhancing their structural performance. Stiffeners are crucial in reinforcing weak areas in CFS members and improve their overall buckling strength and rigidity. Various techniques are employed

E-mail address: dar.adil@sheffield.ac.uk (M.A. Dar).

<sup>\*</sup> Corresponding author.

Nomenc	lature	$M_y$ $P_m$	member yield moment mean value of experimental/FEA-to-predicted moment
The symb	ools used in this study are summarized as follows	r <sub>m</sub>	ratio
$b_f$	width of flange	$r_i$	inner radius of the round corner of sections
$b_1$	depth of lip	$S_f$	gross section modulus referenced to the extreme fiber at
$C_p$	correction factor in reliability analysis	-)	first yield
$f_{DM}(t)$	distribution function for DM section	t	thickness of steel plate with coating
$f_{DOW}(t)$	distribution function for DOW section	$V_F$	coefficient of variation of fabrication factor
$F_m$	mean value of fabrication factor	$V_M$	coefficient of variation of material factor
$f_{y}^{m}$	yield stress	$V_P$	coefficient of variation of experimental/FEA-to- predicted
$h_w$	overall depth of web	- 1	moment ratio
1	width of the overlapped zone	$w_1, w_2$	$w_3$ width of plate elements of stiffened M and Hat sections
$M_{ m crd}$	critical elastic distortional buckling moment	$Z_f$	plastic section modulus
$M_{\rm crl}$	critical elastic local buckling moment	$\beta_0$	target reliability index
$M_{\mathrm{DSM}}$	nominal flexural strength predicted by current DSM	$\beta_1$	reliability index using combination of 1.2 (dead load) and
2011	equations	, -	1.6 (live load)
$M_{ m DSM-G}$	nominal flexural strength predicted by generalized DSM	$\beta_2$	reliability index using combination of 1.25 (dead load) and
2011 0	equations	, _	1.5 (live load)
$M_{\rm EXP}$	moment capacities obtained from experimental	η	(shape/form) coefficient
	investigation	$\overset{\cdot}{ heta}$	angle of inclined web element from the vertical axis
$M_{ m FEA}$	moment capacities obtained from finite-element analysis	$\lambda_d$	slenderness limit for distortional buckling
$M_m$	mean value of material factor	$\lambda_l$	slenderness limit for local buckling
$M_{ m nd}$	nominal flexural strength for distortional buckling	$\lambda_{lf}$	fictive slenderness limit for local buckling
$M_{\rm ne}$	nominal flexural strength for lateral-torsional buckling	$\sigma_{0.2}$	0.2% proof stress (yield stress)
$M_{ m nl}$	nominal flexural strength for local buckling	$\phi_b$	resistance factor for beams
$M_p$	member plastic moment		
•			

for stiffening CFS sections, with intermittent stiffening of webs and flanges being the most widely adopted [6-11]. Additionally, more advanced and intricate stiffening methods involve the use of corrugated webs in built-up sections during high-load situations, as they demonstrate superior performance in preventing buckling failures compared to flat webs [12–16], with triangular web corrugation being more effective than other profiles. Furthermore, other stiffening methods incorporate the use of external stiffeners [17,18], or stiffening materials like concrete [19-21] and lightweight materials like GFRP [22,23], timber [24, 25], cardboard [25], high-density polystyrene [24]. Adopting partial stiffeners takes a different approach by strategically placing stiffening elements to enhance buckling stability in critical areas prone to buckling failure, rather than adopting the stiffener across the entire beam span [17]. Built-up closed sections may precede open sections when torsional rigidity is a primary concern. Efforts to improve torsional rigidity in open sections have included providing transverse gaps between back-to-back channel sections [26,27]. Additionally, specially designed double sigma built-up sections aim to leverage the advantages of both I and box sections through optimised stiffener design within the section [28].

In theoretical analysis of built-up members, it is common to assume double thickness in overlapped zones to simulate the effect of selftapping screws during assembly. This assumption extends to the design of various built-up open and closed sections. The results from the tests conducted on a variety of stiffened sections based on this assumption under flexural loads as reported in [29,30] were compared with design strengths obtained using Direct Strength Method (DSM) [31]. While the DSM offers simplicity by eliminating the need for complex calculations to quantify effective cross-sectional widths, the comparison indicated discrepancies between test strengths and DSM-predicted strengths. As a result, earnest attempts were made to modify DSM equations for their improved predictability, except when the current DSM performs well. The adequacy of modified and current DSM equations was further investigated on more innovative built-up sections, and it was confirmed that the current and modified DSM equations do not predict flexural strengths effectively for closed built-up

sections composed of sigma sections arranged face-to-face [29,32]. This motivated many to investigate such cases further and develop different design equations tailored to various non-conventional built-up sectional profiles, particularly challenging the double thickness assumption. Although, in some evaluations, a section model assumption was made instead of double thickness, yielding good predictions. Instead of modifying the DSM equations, some investigations explored options to change the thickness factor from 2 t (twice thickness) to other factors. The growing number of proposed DSM equations aims to cover a wide range of novel built-up sections. Numerous proposals for DSM equations have also been brought out [33].

One key distinction between CFS single elements and built-up sections lies in the presence of fasteners in the latter. Unlike single elements, which typically do not require any imposed fastening between elements, fasteners play a critical role in built-up sections. They are essential for connecting single-element profiles while maintaining structural integrity and must be considered in the design process. The current North American Specification (NAS) [34], lacks design provisions for conventional built-up sections, making it challenging to determine the required number of fasteners longitudinally and cross-sectionally, especially for unconventional built-up sections. Various studies have attempted to understand the impact of screw spacing on the strength, buckling, and deformation of CFS built-up members, leading to recommendations for minimum fastener spacing. The effect of fastener spacing variation was more pronounced in closed built-up sections due to the presence of fasteners in the compressed flange, which controlled local buckling failure in that region [35]. To ensure efficient contribution of fasteners in enhancing the flexural strength, a minimum fastener spacing is chosen with regards to the local buckling half wavelength of built-up section, obtained from Finite Strip Analysis software (CUFSM) [36]. This helped in bringing out a minimum fastener spacing equal to four times the overall depth of the web [35]. Furthermore, the suitability of adopting a single or double-thickness assumption in overlapped regions for accurate design strengths remains inconsistent. The current DSM equations rely on CUFSM for obtaining elastic critical buckling stress and were primarily developed

for CFS single-element profiles. This reflects the limitation of fastener modelling in CUFSM and, subsequently, the inaccuracy of DSM in predicting the strengths of built-up sections accurately. In a recent study [37], a compound finite strip model was developed to simulate the discretely located fasteners in built-up sections accurately.

This paper discusses the development of a new design method for predicting the flexural strength of built-up sections prone to local buckling failure. Initially, a finite element (FE) model was created in ABAQUS and validated against relevant test results from the literature. The validated FE model was then used to investigate two novel built-up closed sections, DM and DOW sections (explained in detail in the Parametric Study-1 section). Various factors, including cross-sectional dimensions, types of flexural loading, thickness, and fastener spacing, were altered to assess their impact on flexural behaviour. The resulting data was used to evaluate the adequacy of the current DSM for these novel profiles, revealing inconsistencies in their strength predictions. Consequently, a new design method, the Generalised Direct Strength Method (DSM-G), was developed and validated using FE strengths from the current study as well as relevant findings from other studies reported in the literature. DSM-G was validated against six different built-up cross-sectional profiles, comprising a total of 124 data points. A reliability analysis was also conducted to validate DSM-G for all these sections further, reaffirming its versatility and accuracy. The paper concludes with a comprehensive set of guidelines for implementing DSM-G in practical applications along with a design example (see Appendix-I), providing detailed insights for engineers and designers.

### 2. FE modelling technique adopted

The FE Models of open and closed CFS built-up beams from the tests reported in [29] subjected to four-point and three-point bending were replicated using a widely adopted FE-based software ABAQUS [38] commonly used for modelling CFS elements. The test specimens [29] comprised of CFS built-up beams with intermediate stiffeners. The CFS single-element profiles used in constructing the built-up sections were modelled using square-shaped shell elements, namely S4R, available in the ABAQUS software library [38]. This shell element type is popular for accurately modelling CFS sections to replicate their behaviour and is based on reduced integration. Each node of S4R shell element possesses six (three translational and three rotational) degrees of freedom. A convergence study was conducted to determine the optimal size of finite elements, aiming to strike a balance between computational efficiency and the accuracy of FE models. Previous mesh convergence studies on CFS built-up beams have recommended square meshes with dimensions of 5 mm or 10 mm [29,32,35,36]. Consequently, a mesh convergence study was performed on both 5 mm and 10 mm mesh sizes to further refine their appropriateness in aligning with the test results [29]. The load-displacement results of the mesh sensitivity analysis performed on CV-1.0-B4 is depicted in Fig. 1, and the comparisons of flexural strengths are provided in Table 1. Both Fig. 1 and Table 1 indicate that a mesh size of 5 mm yielded more precise results, particularly for the ultra-thin section COW-0.48-B4. Accordingly, this specific mesh size was deemed optimal and subsequently adopted for all specimens. The mechanical and geometrical properties of the FE models were adopted following test data sets reported in the [29]. The actual stress vs. strain data was not reported in the literature [29], only the yield and ultimate strengths were presented. The material behaviour in the FE models was simulated using elasto-plastic material model based on the yield strength and ultimate strength presented in test data [29]. Tables 2 and 3 illustrate the material and geometrical properties of the FE built-up beam models used in the validation component. Various options and procedures are available in ABAQUS [38] that facilitate the effective simulation of the interactions between the components of a built-up section. The interaction between the surfaces in contact was defined prior to the loading application to ensure proper contact and avoid penetration of elements into one another. The hard contact option was adopted to simulate the

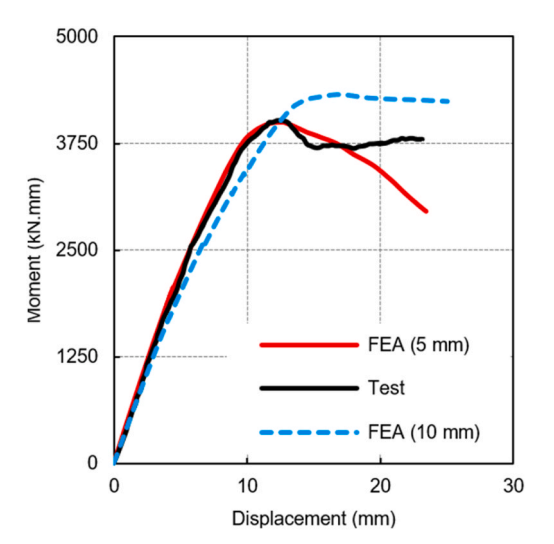


Fig. 1. Results of mesh sensitivity analysis of CV-1.0-B4.

 Table 1

 Comparison of critical bending moment for different mesh sizes.

Sections ID	Mesh size	M <sub>FEA</sub> (KN. mm)	M <sub>Test</sub> (KN. mm)	$ m M_{Test}/  m M_{FEA}$
OV-1.0-B4	$5~mm \times 5~mm$	4427	4238	0.96
	$10~\text{mm}\times10~\text{mm}$	4595		0.92
CV-1.0-B4	$5 \text{ mm} \times 5 \text{ mm}$	3963	4088	1.03
	$10~\text{mm}\times10~\text{mm}$	4319		0.95

normal behaviour and a frictionless option was chosen to model the tangential behaviour. Since the sliding between the elements in contact is small, the small sliding approach was selected. Further, this option is computationally efficient when compared to finite sliding formulations. The adjustment tolerance was chosen to be slightly greater than the thickness of the section to accommodate for any possible numerical errors of the nodal coordinates in the FE model. The screw connections in overlapped zones were simulated by using the mesh-independent fastener option available in ABAQUS library [38]. Attachment points located in the master and slave surfaces were adopted for the screw connections instead of physical modelling of the screws, as no screw failure was reported in tests [29]. Geometrical imperfections are critical in thin-walled sections and must be considered carefully in the FE modelling for predicting the behaviour accurately and reliably. The cross-sectional level imperfections (local imperfections) and the member-span level imperfections (global imperfections) need to be considered. Hence, to incorporate both these types of imperfections into the FE model, a buckling analysis was carried out to determine the relevant buckling modes critically governing the behaviour of the built-up beams under consideration. The buckling modes were presented as eigenmodes, scaled into the model, with a value corresponding to the geometric imperfection value of 0.34 xt as recommended by Schafer and Pecoz [39]. Fig. 2 presents the first Eigenmode (representing the local imperfection) obtained from the buckling analysis on OW-1.0-B4 specimen [29]. The coupling constraints option was chosen to simulate the hinge and the roller support for replicating the simply supported boundary condition. Two reference points, namely RP1 and RP2 were created at geometrical centroids of the beam ends, which were connected to the edges of the beam cross-section using multi-point constraints, as shown in Fig. 3. The reference points RP1 and RP2 were restrained in all degrees of freedom (DOF's), except that UR1 (rotation about X axis) was released at RP1 to simulate the hinge boundary condition, and U3 and UR1 were released at RP2 to simulate the roller boundary condition. RP3 and RP4 were the reference points created at the sectional geometrical centroids vertically under the

 Table 2

 Geometrical properties of the validated beams [29].

Specimen	b <sub>l</sub> (mm)	b <sub>f</sub> (mm)	h <sub>w</sub> (mm)	w <sub>1</sub> (mm)	w <sub>2</sub> (mm)	w <sub>3</sub> (mm)	t	t * (mm)	R (mm)
OV-1.0-B4	-	53.7	85.6	26.5	22.2	-	1.041	1.003	3.5
OI-1.0-B4	14.5	29.9	98.4	25.9	26.7	17.1	1.028	0.986	3.4
CV-1.0-B4	-	52.1	85.6	27.3	22.7	-	1.046	1.008	3.3
CV-0.48-B4	-	53.7	85.7	26.2	24.2	-	0.565	0.475	3.5
COW-1.0-B4R	-	50.2	70.9	15.7	16.7	43.9	1.066	1.020	3.5
COW-0.48-B4	-	50.6	69.4	14.7	15.6	42.8	0.575	0.475	3.8
COF-1.0-B4	-	51.9	70.2	15.0	15.4	44.8	1.065	1.019	3.5
COF-0.48-B4	-	50.6	69.4	14.7	15.6	42.8	0.575	0.475	3.8
COW-1.0-B3	-	50.0	72.1	14.6	16.4	45.5	1.058	1.012	3.5

**Table 3**Mechanical properties of the validated beams.

Section	E (GPa)	σ <sub>0.2</sub> (MPa)	σ <sub>u</sub> (MPa)	$\varepsilon_{\mathrm{f}}$ (%)
CV-0.48	213	661	690	2.0
OV-1.0/CV-1.0	213	598	599	9.7
COF-0.48/COW-0.48	214	662	707	1.8
COF-1.0/COW-1.0	216	572	583	9.6
OI-1.0	216	592	599	8.6

loading points and were similarly connected to the edges of the built-up section. This ensured that the adjacent surfaces are restrained to avoid web crippling caused by loading concentration while simulating the infilled wooden blocks. RP5 and RP6 were created at the centroid of the thick loading plates located at the upper flanges. They were connected to RP3 and RP4, respectively, to effectively transfer the load to the specimen during the loading process while mimicking the rigid body motion of the loading plates. ABAQUS [38] facilitates introducing nonlinearities in the FE model through geometric, material, and boundary conditions. Hence, selecting a nonlinear solution based on Newton-Raphson iteration is not sufficient to attain convergence, which is highly affected by contact options, finite element mesh type and size, and the nature of the problem dealing with local and global instabilities. Due all to these considerations, the task of creating a cohesive numerical model that encompasses all the mentioned aspects proved to be a tedious task. As a result, many convergence issues were encountered, leading to premature termination of the analysis before reaching the ultimate stress. Additionally, the analysis required a significant amount of time to complete. However, these issues were effectively resolved by increasing the number of increments and incorporating artificial damping with a default value of 0.0002 in the nonlinear step. This served to prevent the loss of rigidity in contact regions, which often results in premature termination of the analysis. Moreover, a preliminary general static step was defined before the main step, aimed to gradually apply small displacements to the model, facilitating the establishment of contact between the individual parts of the specimen. These adjustments worked

synergistically to avoid convergence issues and ensure the successful completion of the analysis.

#### 3. Validation of FE model

Validation of FE models against the test results is crucial in acquiring the desired reliability in the FE models to be extendable to parametric studies. Accordingly, the FE models developed as discussed in the previous section, were verified against all the tests (a total of 9) conducted by Wang Young [29]. All 9 built-up open and closed sections (OV, COW, CV, and COF) experiencing four-point and three-point bending were considered. The details about these built-up sections will be detailed in the design section. The geometric and material properties adopted are detailed in Tables 2 and 3. Table 4 illustrates the peak strength validation of the specimens, showing a good agreement between the maximum bending moment obtained from tests and FE analyses, with a mean flexural strength ratio  $M_{\text{Exp}}/M_{\text{FEA}}$  of unity and a standard deviation of 0.58. Fig. 4 depicts the failure prediction accuracy of the FE models by comparing the deformed shapes (FE analyses vs. tests) for specimens CV-1.0-B4, COW-1.0-B4 and COF-1.0-B4 upon reaching the maximum bending moment. To further support the accuracy of our FE models, the moment-displacement response and moment-curvature curves (FE analyses vs. tests), for specimens CV-1.0-B4, COW-1.0-B4, and OV-1.0-B4 are presented in Fig. 5. By comparing the outcomes (FE analyses vs. tests) on all three fronts (peak strengths, failure modes, and strength-displacement characteristics), we reliably verified the adequacy of our FE models to be fit for the intended parametric study to be discussed in the next section.

### 4. Parametric study-I (Altering the screws arrangements)

Generally, the studies that primarily examine the influence of screw spacing on the strength and failure of built-up members are independent of their structural design. However, it is crucial to recognise that the design rules governing the capacity of built-up sections rely on several

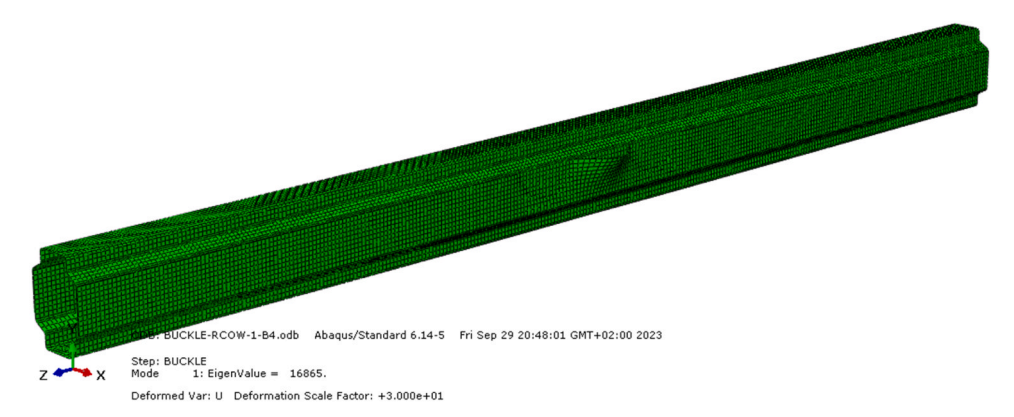


Fig. 2. First Eigenmode obtained from the buckling analysis of COW-1.0-B4 [29].

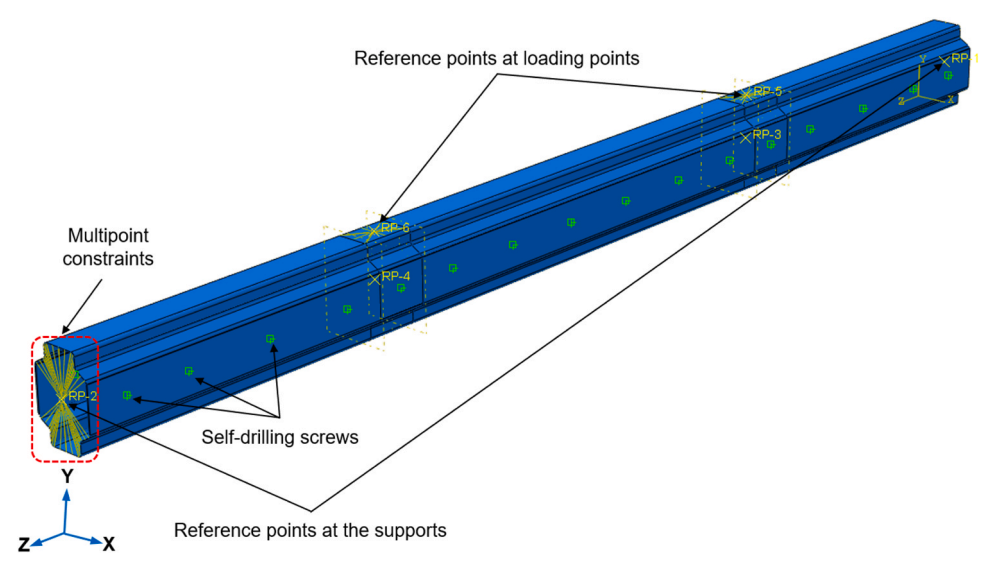


Fig. 3. Modelling details of loading, boundary condition and fasteners.

assumptions concerning the overlapped zones where screws are placed. Consequently, considering the effect of screws spacing becomes imperative when determining the convenient approach, either employing the double thickness assumption in overlapped zones or considering the strength of a built-up member as the sum of two individual sections, Additionally, a recent study conducted by [37] introduced a method to directly model discrete fasteners by incorporating their stiffness into the global stiffness matrix of the member in Finite Strip analysis. By factoring in screw spacing during this decision-making process, a more comprehensive and accurate assessment of built-up sections performance can be achieved.

In the present NAS [34] the screw spacing requirements have only been recommended for back-to-back built-up beams with a maximum permissible longitudinal spacing of span/6. For built-up face-to-face connected members, diligent attempts were made to obtain the optimal screw spacing values, and a maximum spacing equal to four times the web height was proposed [35]. The validated FE model was used to investigate the behaviour of 52 beams under four-point bending (27 for DM and 25 for DOW sections), Fig. 6 and Table 5 provide the dimensional properties of built-up sections DM and DOW, adopted in the current study. The novel built-up sections comprise of overlap zones located at the web, serving dual roles as stiffeners and assembly points,

**Table 4**Comparison between deformed shapes and maximum bending strengths (MTest vs. MFEA).

Specimens	Tests[29] M <sub>Test</sub> (kN.mm)	Failure modes	FEA M <sub>FEA</sub> (kN.mm)	Failure modes	Comparison $M_{Test}/M_{FEA}$
OV-1.0-B4	4238	L+F	4427	L+F	0.96
OI-1.0-B4	6092	D+F	6037	D+F	1.01
CV-1.0-B4	4088	L+F	3963	L+F	1.02
CV-0.48-B4	1266	L+F	1301	L+F	0.97
COW-1.0-	4730	L+F	4810	L+F	0.98
B4					
COW-0.48-	1699	L+F	1780	L+F	0.95
B4					
COF-1.0-B4	3749	L+F	3547	L+F	1.06
COF-0.48-	1278	L+F	1168	L+F	1.09
B4					
COW-1.0-	5181	L+F	5494	L+F	0.94
В3					
Mean					1.00
Standard devi	iation				0.58

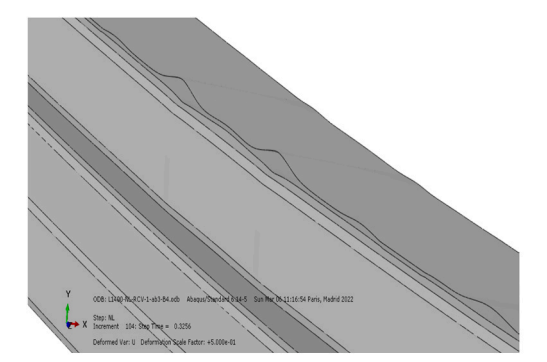
Note: L: Local Buckling; D: Distortional Buckling; F: Flexural Buckling

ultimately creating fully-stiffened built-up sections. The nomenclature assigned to these novel sections was derived from their distinctive sectional shapes. Specifically, "DM" denotes Double 'M' sections (refer to Fig. 6(a)), while "DOW" designates Double sections forming an overall circular shape resembling an 'O' with 'W'-shaped stiffeners (refer to Fig. 6(b)). The material properties employed for all specimens were derived from ones reported in [29], specifically in accordance with COF-1.0/COW-1.0 sections, as presented in Table 3. A total of 52 beam models (27 for DM and 25 for DOW) were investigated for the influence of screws spacing under four and three-point bending, taking into consideration the following details, (i) the longitudinal screw spacing altered in the bending span only, (ii) the longitudinal screw spacing varied along the entire beam span at the intervals of span/2, span/4, span/8 and span/20, this was to primarily cover the influence of screw spacing on the strength and failure modes of the specimens. (iii) variably altering the screw spacing values for beams with different spans to cover short, intermediate, and long beams. The following beam spans have been adopted: 900, 1400, 2500, and 3500 mm. The nomenclature used for the specimens was in accordance with the critical parameters like section label, thickness, and beam span, screw spacing. For example, in the label 15-DM-S600-1.0-L1400, 15-DM refers to the section label, 1.0 is the thickness, \$600 is the screw spacing in the bending moment span, and L1400 is the span of the specimen.

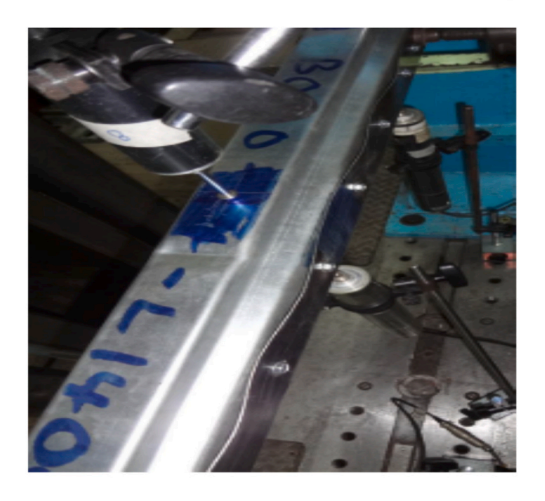
# 5. Parametric study-II (Altering the cross-sectional characteristics)

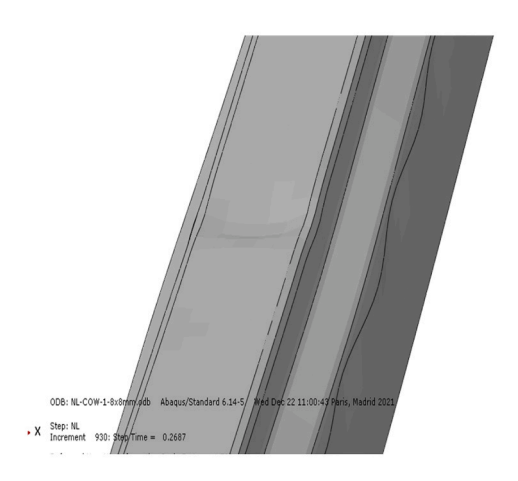
Many parameters were varied throughout the parametric study-II analysis, including the cross-sectional profiles and sectional slenderness of the element's plate, the type of loading i.e., four-point and threepoint bending, resulting in a total of 56 (32 for DM and 24 for DOW) beams models being investigated. To understand the influence of crosssectional variation on the structural behaviour of the two novel sections, two different span values (1400 mm and 2500 mm) were adopted. The deliberate variation in span aimed to influence the specimen's behaviour by extending the moment span, potentially altering the member slenderness, thereby affecting the possibility of local buckling failure. The current investigation focused on studying the moment capacities and failure shapes of six sections, with three sections for DM and three sections for DOW. Each section varied in thickness, ranging from 0.30 to 2.4 mm. The minimum thickness employed in this study fulfilled the requirements and limits outlined in Tables B4.1-1 [34], which stipulated a maximum flat width-to-thickness ratio (w/t) < 500 for cases





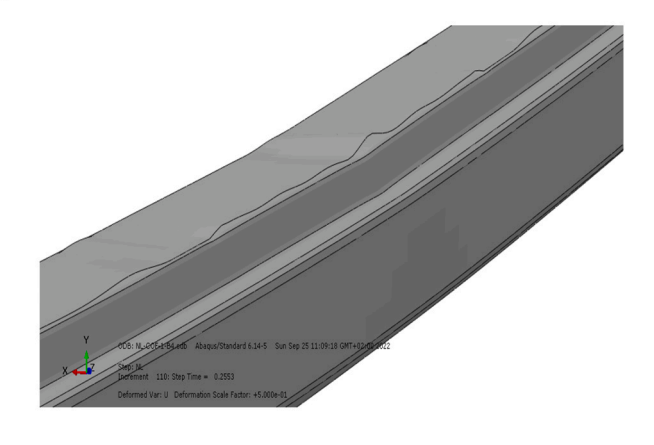
a) For CV-1.0-B4 section





b) For COW-1.0-B4





c) For COF-1.0-B4

Fig. 4. Comparison of failure modes from test and FE modelling.

involving stiffened flanges connected to stiffened webs via edge stiffeners. Additionally, a height-to-thickness ratio (h/t) < 300 was verified to prevent excessive deformation under design loads. It must be noted that parametric study-II was carried out mainly to assess the design strengths predicted by various design rules. Therefore, the results of parametric study-II will be discussed in the design rules section.

### 6. Results from parametric study-I

Tables 6 and 7 summarise the effect of screw spacing on the maximum FEA bending moments predicted and the corresponding

deformed failure shapes of the DM and DOW specimens, respectively. The results suggest that both DM and DOW sections exhibited a comparable response to variation in screw spacing. In general, it was noted that the screw spacing did not affect the bending strength or deformed failure shapes, except in cross-sectionally slender specimens with \$1000 screw spacing arrangement, where the overlapped zone underwent a separation between the individual elements (due to compatibility issue in the cross-sectional geometry), as shown in Fig. 7(a&b), for specimens 17-DM-\$1000-L2500-0.38-B4 and 17-DOW-\$1000-L2500-0.48-B4, respectively. For all specimens, local buckling in the upper part of the compression zone (experiencing higher compressive stresses) was the

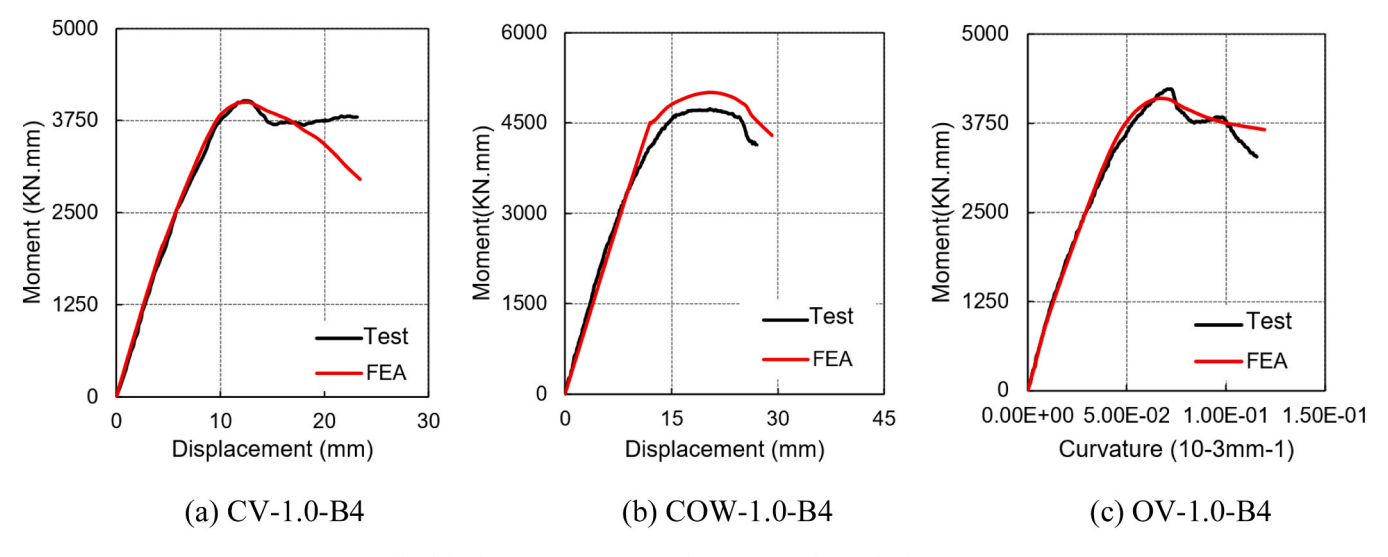


Fig. 5. Comparison of load-displacement curves, (a) & (b) moment-mid-span displacement, (c) moment-curvature.

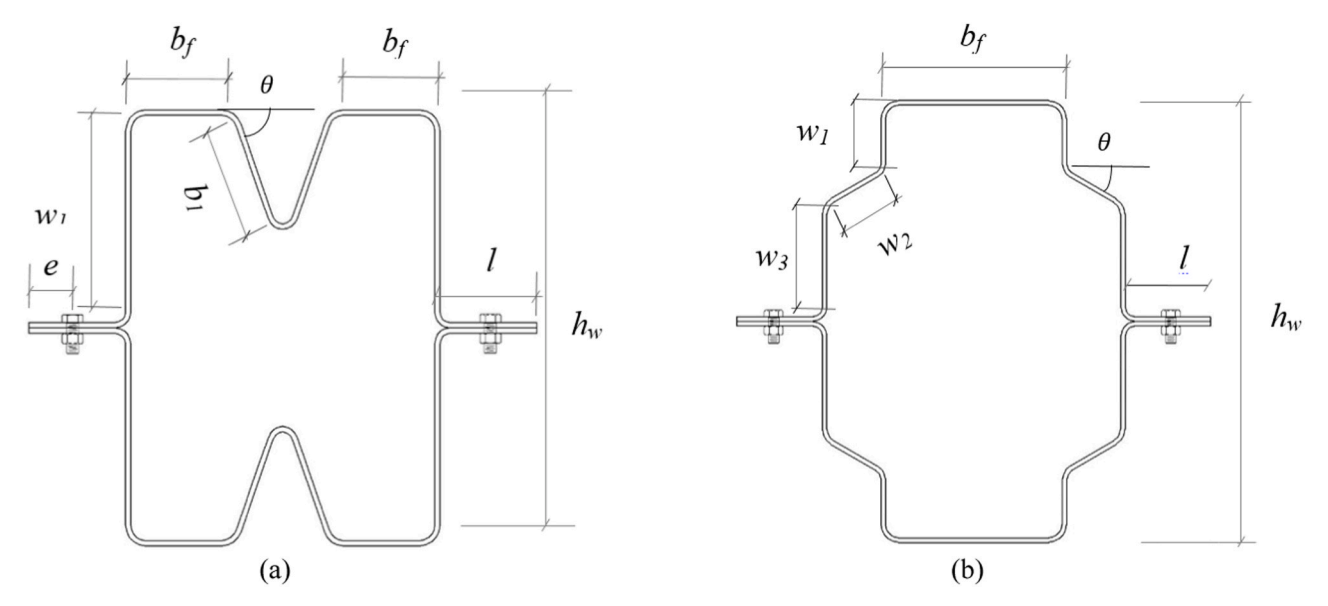


Fig. 6. Geometrical properties of built-up sections: a) DM, b) DOW.

**Table 5**Dimensional properties of DM and DOW sections.

Specimen	h <sub>w</sub> (mm)	b <sub>f</sub> (mm)	b <sub>1</sub> (mm)	w <sub>1</sub> (mm)	W <sub>2</sub> (mm)	w <sub>3</sub> (mm)	L (mm)	θ (°)	e (mm)
DM	82.00	40.72	23.25	39.42	-	-	19.51	70	8.50
15-DM	83.00	37.20	14.22	39.92	-	-	19.51	30	8.50
17-DM	122.00	42.28	23.29	59.41	-	-	19.50	70	8.50
DOW	98.29	41.52	-	15.25	14.68	24.86	19.50	30	8.50
15-DOW	84.95	41.00	-	15.43	11.24	24.72	19.5	0	8.50
17-DOW	126.04	41.00	-	15.72	25.94	23.16	19.5	60	8.50

dominant failure mode observed. However, in specimens with wall thickness under 1 mm, an interaction between local and distortional buckling was noticed. Additionally, the impact of the screw spacing variation on the bending strengths in the ultra-thin sections was higher due to their sensitivity towards buckling failure compared to the stockier ones. Also, the type of loading (three-point/four-point bending) had a meagre on the bending strength and failure shapes when the screw spacing was varied. Moreover, a minimum screw requirement, especially within the bending span, is essential to prevent any detachment

between individual components. The consideration for local buckling half wavelength obtained from CUFSM Software [36] as shown in Fig. 8 (a&b) for specimens DM-2.4 & 17-DOW-2.4 is not accounted for. Subsequently, this outcome favours the adequacy of the double-thickness approach along with its simplicity in adoption while designing such built-up sections. Moreover, this study cannot opt for a monolithic sectional model assumption due to the asymmetry of the individual elements about their bending axis, as shown in Fig. 6(a&b). This lack of symmetry renders considering the strength of the built-up section as the

**Table 6**Influence of screws spacing on the flexural strength and deformed shapes of DM sections.

Specimens	M <sub>FEA</sub> (kN. mm)	Failure mode	Specimens	M <sub>FEA</sub> (kN. mm)	Failure mode
17-DM-S125- L2500-1-B4	7989	L+Y	15-DM-L/2- L1400-0.30- B4	873	L+D+Y
17-DM- S338- L2500-1-B4	7927	L+Y	15-DM-S90- L1400-1-B4	4282	Y
17-DM-S1000- L2500-1-B4	7924	L+Y	15-DM-S300- L1400-1-B4	4235	Y
17-DM-L/20-	8028	L+Y	15-DM-S600-	4224	Y
L2500-1-B4 17-DM-L/2- L2500-1-B4	7966	L+Y	L1400-1-B4 15-DM-L/20- L1400-1-B4	4267	Y
17-DM-S125- L2500-0.38- B4	2145	L+D+Y	15-DM-L/8- L1400-1-B4	4267	Y
17-DM-S338- L2500-0.38- B4 17-DM- S1000- L2500-0.38- B4	2069 1282	L+D+Y L+D+SP+Y	15-DM-L/2- L1400-1-B4 DM-S90- L1400-0.48- B4	4245 1897	Y L
17-DM-L/20- L2500-0.38- B4	2200	L+D+Y	DM-S300- L1400-0.48- B4	1832	L+D
17-DM-L/8- L2500-0.38- B4	2111	L+Y	DM-S600- L1400-0.48- B4	1769	L+D
17-DM-L/2- L2500-0.38- B4	1942	L+Y	DM-L/20- L1400-0.48- B4	1948	L+Y
15-DM-S90- L1400-0.3- B4	1203	L+D+Y	DM-L/8- L1400-0.48- B4	1937	L+Y
15-DM-S300- L1400-0.3- B4	977	L+D+Y	DM-L/2- L1400-0.48- B4	1813	L+Y
15-DM-S600- L1400-0.3- B4	920	D+L+Y	17-DM-S100- L3500-1-B3	8620	Y+L
15-DM-L/20- L1400-0.30- B4	1071	L+D+Y	17-DM-S425- L3500-1-B3	8638	L+Y
15-DM-L/8- L1400-0.30- B4	1006	D+L+Y	17-DM- S1137- L3500-1-B3	8651	L+Y

Note: L: Local Buckling; D: Distortional Buckling; Y: Yielding; SP: Individual sections separation

sum of the individual sections inappropriate.

### 7. Design rules

In the initial attempts to establish design rules for built-up CFS sections, Effective Width Method (EWM), initially developed for CFS individual elements, was used to analyse built-up members. However, the complexity of the cross-sectional shape, particularly for stiffened sections, added to the laborious calculations of effective widths, which led to the development of the Direct Strength Method (DSM). DSM serves as an alternative to EWM and aims to directly determine the nominal strength of the sections by suggesting a possible elastic buckling failure under flexural strength, such as  $M_{crb}\,M_{crd}$  and  $M_{c\,re}$ , without the need to treat each cross-sectional plate element individually as required in EWM. The equations proposed in DSM are based on experimental data, Generalized Beam Theory, and signature curves derived from buckling analysis using Finite Strip Method software CUFSM [36]. The minimum points in these curves indicate the critical buckling load causing local, distortional or global buckling.

**Table 7**Influence of screws spacing on the flexural strength and deformed shapes of DOW sections.

Specimens	M <sub>FEA</sub> (kN. mm)	Failure mode	Specimens	M <sub>FEA</sub> (kN. mm)	Failure mode
17-DOW- S1000- L2500-1-B4	5262	D+Y	15-DOW- S1000-L2500- 1-B4	3818	D+Y
17-DOW -S134- L2500-0.48- B4	3137	L+D+Y	15-DOW-S90- L1400-1-B4	4053	Y
17-DOW- S333- L2500-0.48- B4	2469	L+D+Y	15-DOW- S600-L1400- 1-B4	3978	Y
17-DOW- \$1000- L2500-0.48- B4	2855	L+D+SP+Y	17-DOW-S90- L2500-1-B3	6411	L+Y
17-DOW-L/ 20-L2500- 0.48-B4	2960	D+L+Y	DOW-S90- L1400-0.30- B4	1076	L+D+Y
17-DOW-L/8- L2500-0.48- B4	2886	L+D+Y	DOW-S600- L1400-0.30- B4	1065	L+D+Y
17-DOW-L/2- L2500-0.48- B4	2509	L+D+Y	DOW-L/2- L1400-0.30- B4	1068	L+Y
15-DOW- S82.5-L900- 1-B4	4064	Y	17-DOW- S430-L2500- 1-B3	6205	L+Y
15-DOW- S400-L900- 1-B4	4076	Y	17-DOW- S1100-L2500- 1-B3	6113	L+Y
15-DOW- S82.5-L900- 0.3-B4	1305	L+Y	17-DOW-S90- L2500-0.48- B3	2658	L+Y
15-DOW- S400-L900- 0.3-B4	1021	L+Y	17-DOW- S430-L2500- 0.48-B3	2474	L+Y
15-DOW- S125- L2500-1-B4	3984	Y+D	17-DOW- S1100-L2500- 0.48-B3	2406	L+Y

Note: L: Local Buckling; D: Distortional Buckling; Y: Yielding; SP: Individual sections separation.

In this study the proposed built-up sections were regarded as fully braced to prevent the occurrence of lateral torsional buckling. As a result, the nominal flexural strength  $(M_{ne})$  for lateral-torsional buckling is equal to the yield moment capacity  $(M_y)$ , while anticipating the section's failure by either local or distortional buckling. The DSM flexural buckling strengths can be obtained from the expressions summarised as follows:

$$M_{nl} = \left\{ \begin{aligned} M_{y} + \left(1 - \frac{1}{C_{yl}^{2}}\right) \left(M_{p} - M_{y}\right) & for \quad \lambda_{l} \leq 0.776\\ \left[1 - 0.15 \left(\frac{M_{crl}}{M_{y}}\right)^{0.4}\right] \left(\frac{M_{crl}}{M_{y}}\right)^{0.4} M_{y} & for \quad \lambda_{l} > 0.776 \end{aligned} \right\}$$
(1)

$$M_{nd} = \left\{ M_{y} + \left(1 - \frac{1}{C_{yl}^{2}}\right) (M_{p} - M_{y}) \quad for \quad \lambda_{l} \leq 0.673 \\ \left[1 - 0.22 \left(\frac{M_{crl}}{M_{y}}\right)^{0.5}\right] \left(\frac{M_{crl}}{M_{y}}\right)^{0.5} M_{y} \quad for \quad \lambda_{l} > 0.673 \end{cases} \right\}$$
(2)

Where  $\lambda_l = \sqrt{\frac{M_y}{M_{crl}}}; C_{yl} = \sqrt{\frac{0.776}{\lambda_l}} \leq 3; M_y = f_y S_f; M_p = Z_f f_y; S_f = \text{gross}$  section modulus referenced to the extreme fiber at first yield;  $Z_f = \text{plastic}$  section modulus;  $f_y = \text{yield}$  stress, which is the 0.2% proof stress  $(\sigma_{0.2})$ 

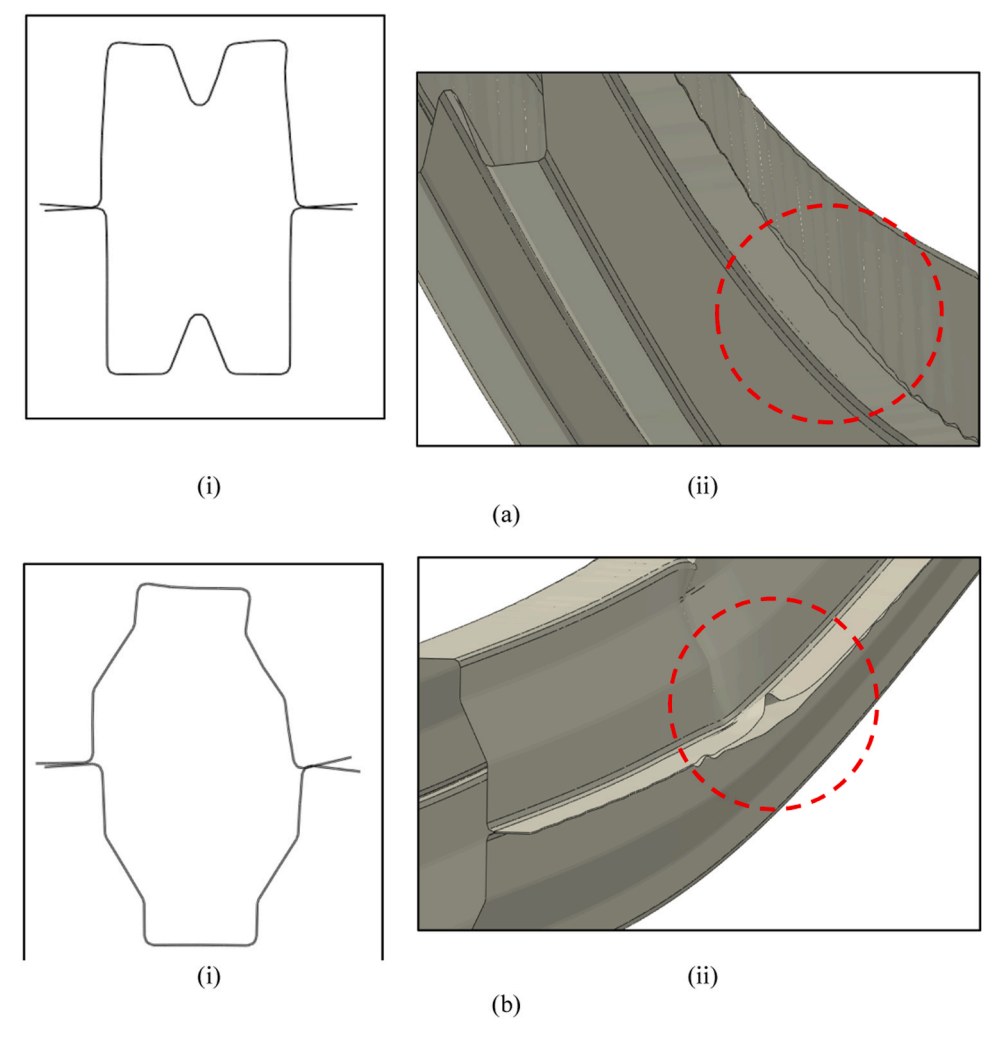


Fig. 7. Failure shapes for specimens (a) 17-DM-S1000-L2500-0.38-B4, (b) 17-DOW-S1000-L2500-0.48-B4; (i): cross-sectional view, (ii): longitudinal view.

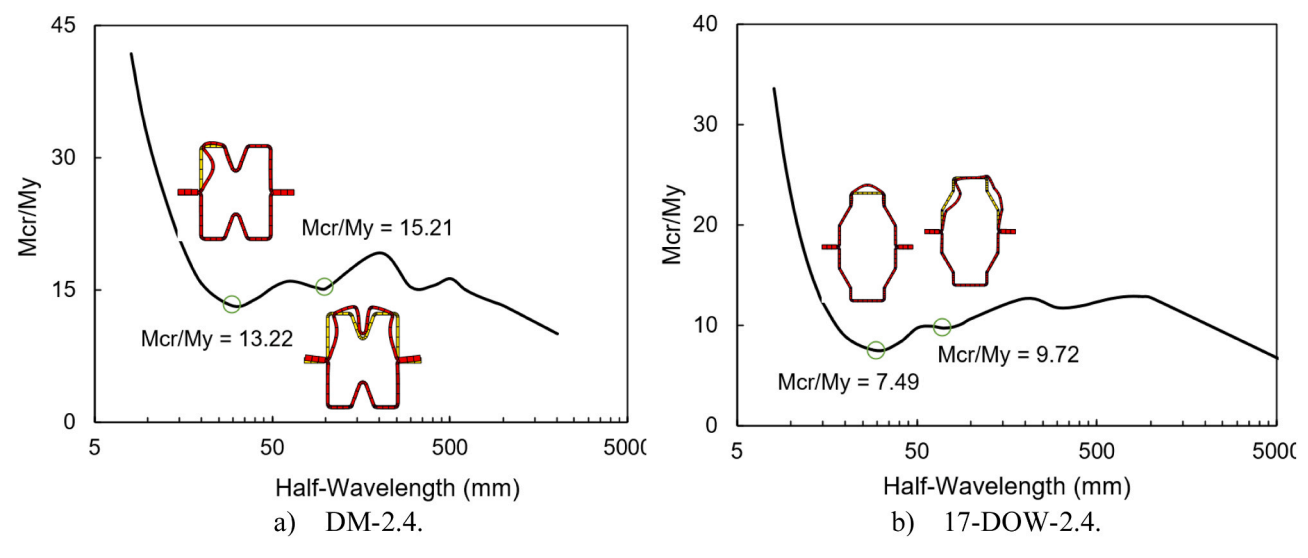


Fig. 8. Signature curve using CUFSM software [36] for: (a) DM-2.4, (b) 17-DOW-2.4 sections.

obtained from tensile coupon tests in this study;  $M_{crl}=$  critical elastic buckling moment obtained from CUFSM signature curve,  $\lambda_d=\sqrt{\frac{M_y}{M_{crd}}}$ ;  $C_{yd}=\sqrt{\frac{0.673}{\lambda_d}}\leq 3$ ; and  $M_{crd}=$  critical elastic distortional buckling moment

obtained from CUFSM signature curve.

 $M_{DSM}$  is regarded as the minimum of nominal flexural strength for local  $M_{nl}$  and distortional buckling  $M_{nd}$ :

$$M_{DSM} = \min(M_{nl}; M_{nd}) \tag{3}$$

**Table 8**Maximum bending strength comparison (FEA vs. DSM) for DM sections.

S.No	Specimen	M <sub>FEA</sub> (kN.mm)	$\lambda_{l}$	$\lambda_{\mathbf{d}}$	M <sub>nl</sub> (kN.mm)	M <sub>nd</sub> (kN.mm)	$M_{FEA}/M_{DSM}$
1	DM-2.4	12434	0.28	0.26	11355	11280	1.10
2	DM-1.5	7517	0.43	0.32	6681	6808	1.13
3	DM-1.0	4881	0.64	0.40	4202	4450	1.16
4	DM-0.7	3094	0.89	0.47	2631	3101	1.18
5	DM-0.6	2452	1.04	0.51	2050	2622	1.20
6	DM-0.5	1935	1.23	0.56	1524	2061	1.27
7	DM-0.48	1904	1.28	0.57	1398	2017	1.36
8	DM-0.40	1544	1.51	0.46	1061	1787	1.46
9	DM-0.3	977	1.96	0.73	651	1174	1.50
10	15-DM-2.4	11101	0.34	0.26	10049	10163	1.10
11	15-DM-1.5	6688	0.45	0.44	6145	6053	1.09
12	15-DM-1.0	4282	0.64	0.79	3913	2000	1.09
13	15-DM-0.7	2805	0.90	0.99	2427	1634	1.16
14	15-DM-0.6	2248	1.05	0.89	1882	1182	1.19
15	15-DM-0.5	1759	1.23	0.54	1409	1984	1.25
16	15-DM-0.48	1740	1.28	0.55	1317	1898	1.32
17	15-DM-0.40	1491	1.52	0.47	973	1618	1.53
18	15-DM-0.30	1203	2.00	0.68	602	1142	2.00
19	17-DM-2.4	22230	0.40	0.37	19621	19461	1.14
20	17-DM-1.5	13296	0.63	0.42	11515	12051	1.15
21	17-DM-1.0	8253	0.94	0.40	6533	8151	1.26
22	17-DM-0.7	4903	1.32	0.60	3643	5330	1.35
23	17-DM-0.6	4259	1.54	0.51	2810	4716	1.52
24	17-DM-0.5	3577	1.86	0.46	2054	4012	1.74
25	17-DM-0.48	3017	1.92	0.57	1922	3695	1.57
26	17-DM-0.40	$2379^{2}$	2.29	0.63	1412	3022	1.69
27	17-DM-0.38	2250	2.43	0.73	1288	2279	1.75
Mean	_	_	_	_	_	_	1.34
COV	_	_	_	_	_	_	0.18
Reliability is	$ndex \beta_1$	_	_	_	_	_	3.58
Reliability is	$ndex \beta_2$	_	_	_	_	_	3.75

Table 9
Maximum bending strength comparison (FEA vs. DSM) for DOW sections.

S.No	Specimen	M <sub>FEA</sub> (kN.mm)	$\lambda_{l}$	$\lambda_{\mathbf{d}}$	$M_{nl}$ (kN.mm)	$M_{nd}$ (kN.mm)	$M_{FEA}/M_{DSM}$
1	DOW-2.4	12662	0.37	0.25	11094	11379	1.14
2	DOW-1.5	7714	0.58	0.43	6525	6717	1.18
3	DOW-1.0	4544	0.86	0.55	3818	4301	1.19
4	DOW-0.7	2565	1.22	0.48	2138	3104	1.20
5	DOW-0.6	2160	1.43	0.69	1647	2786	1.31
6	DOW-0.5	1995	1.69	0.43	1219	2257	1.64
7	DOW-0.48	2094	1.77	0.79	1135	1813	1.85
8	DOW-0.40	1312	2.09	0.62	840	1685	1.56
9	DOW-0.3	1046	2.77	0.98	511	983	2.05
10	15-DOW-2.4	10596	0.36	0.76	9336	7513	1.41
11	15-DOW-1.5	6421	0.57	3.02	6248	5029	1.28
12	15-DOW-1.0	4053	0.30	0.65	4024	3472	1.17
13	15-DOW-0.7	2242	1.40	0.60	1643	2496	1.36
14	15-DOW-0.6	2152	1.67	1.37	1247	1274	1.73
15	15-DOW-0.5	1522	2.13	0.81	871	1564	1.75
16	15-DOW-0.4	1263	3.16	0.63	660	1763	1.91
17	15-DOW-0.3	948	2.24	2.67	506	359	2.64
18	17-DOW-2.4	16139	0.37	0.32	11991	12004	1.35
19	17-DOW-1.5	9797	0.58	0.41	9008	9340	1.09
20	17-DOW-1.0	5997	0.86	0.44	5264	6180	1.14
21	17-DOW-0.7	3595	1.21	0.68	2949	3941	1.22
22	17-DOW-0.6	3001	1.41	0.56	2276	3551	1.32
23	17-DOW-0.5	2730	1.67	0.49	1690	3046	1.62
24	17-DOW-0.4	2238	2.09	0.44	1152	2486	1.94
25	17-DOW-0.3	1158	2.67	0.73	721	1631	1.61
Mean		_	_	_	_	_	1.51
COV		_	_	_	_	_	0.24
Reliability is	ndex b1	_	_	_	_	_	3.42
Reliability is	ndex b2	_	_	_	_	_	3.58

### 8. Reliability analysis

Reliability analysis must be compulsorily carried out to verify the adequacy of any design criterion. The design rule is deemed probabilistically safe when the computed reliability index  $(\beta)$  surpasses the

specified target reliability index  $\beta_0$ . For structural elements designed as per Load and Resistance Factor Design (LRFD), a target reliability index of 2.5 is recommended in the analysis, as discussed in Section K.2.1.1 of [34]. A resistance factor  $(\varphi_b)$  of 0.8 was employed in accordance with Section A1.2 (c) of [34]. The load combinations used were (1.2 DL + 1.6 LL) as recommended in [40], and (1.25 DL+1.5 LL) as outlined in [41],

where DL stands for the dead load and LL for live load. A dead-to-live load ratio of 1/5 was employed, as mentioned in section Section K.2.1.1 of [34].

Statistical parameters for the bending strength assessment of beams were sourced from Table K.2.1.1–1 of [34]. The mean for material factor  $(M_m=1.10)$ , fabrication factor  $(F_m=1.00)$ , coefficients of variation  $(V_M=0.10,\ V_F=0.05)$ , and statistical parameters  $P_m$  and  $V_P$  were incorporated. A correction factor  $(C_P)$  was introduced into the reliability assessment to accommodate the effect of a restricted dataset, as per Sections K2.1.1–4 of the same source [34]. The computation of the reliability index  $(\beta 1)$  involved  $(1.2\ DL+1.6\ LL)$  load combination, while the reliability index  $(\beta 2)$  employed  $(1.25\ DL+1.5\ LL)$  load combination.

### 9. DSM predictions

The accuracy of the current design DSM Eq. (1) and (2), in predicting the flexural strength for DM and DOW sections is reported in Tables 8 and 9, respectively. The maximum FEA flexural strengths ( $M_{FEA}$ ) were compared to the DSM-based nominal flexural strengths ( $M_{DSM}$ ). For DM and DOW, the mean values of the bending strength ratio  $M_{FEA}/M_{DSM}$  were 1.34 and 1.51, respectively. The coefficients of variation (COV) for DM and DOW were 18% and 24%, respectively, reflecting a high variation in the predictions. These results indicate that the current DSM equations underestimate the flexural capacity of the built-up sections, making them overly conservative in predicting the flexural strengths. This prediction underestimation could be due to the unconventional cross-sectional shape adopted in the current study. Unlike most built-up

sections, connected by assembling channel or sigma sections, the proposed sections are based on other forms, such as the double M section (DM). The double thickness assumption could also present another constraint in accurately predicting the strength and the actual deformed shape. As noted previously, the screws spacing analysis showed a minor impact of spacing on the flexural strengths.

# 10. Modified DSM proposed for built-up sections and their predictions

The DSM in its current form was developed initially for lipped channel sections (single element profiles) and lacks specific design rules for built-up members as they have not been adequately addressed. This becomes the primary limitation of this design method despite being simpler to adopt. The assembling in built-up sections at discreet locations to meet the specific structural requirements makes capturing their complex behaviour difficult. Therefore, it affects the strength-predicting accuracy in the original DSM equations. As a result, many modified DSM equations have been proposed to capture the complex behaviour of built-up sections when the current DSM fails to do so. However, these modifications were made while only investigating a few sectional profiles [28,32]. Following are some examples of the modified DSM equations proposed for built-up sections:

For built-up closed sections failed in local buckling, Eq. (4) and (5) predicted the flexural strength of sections names as CV/COF and COW, respectively as in [30] investigation:

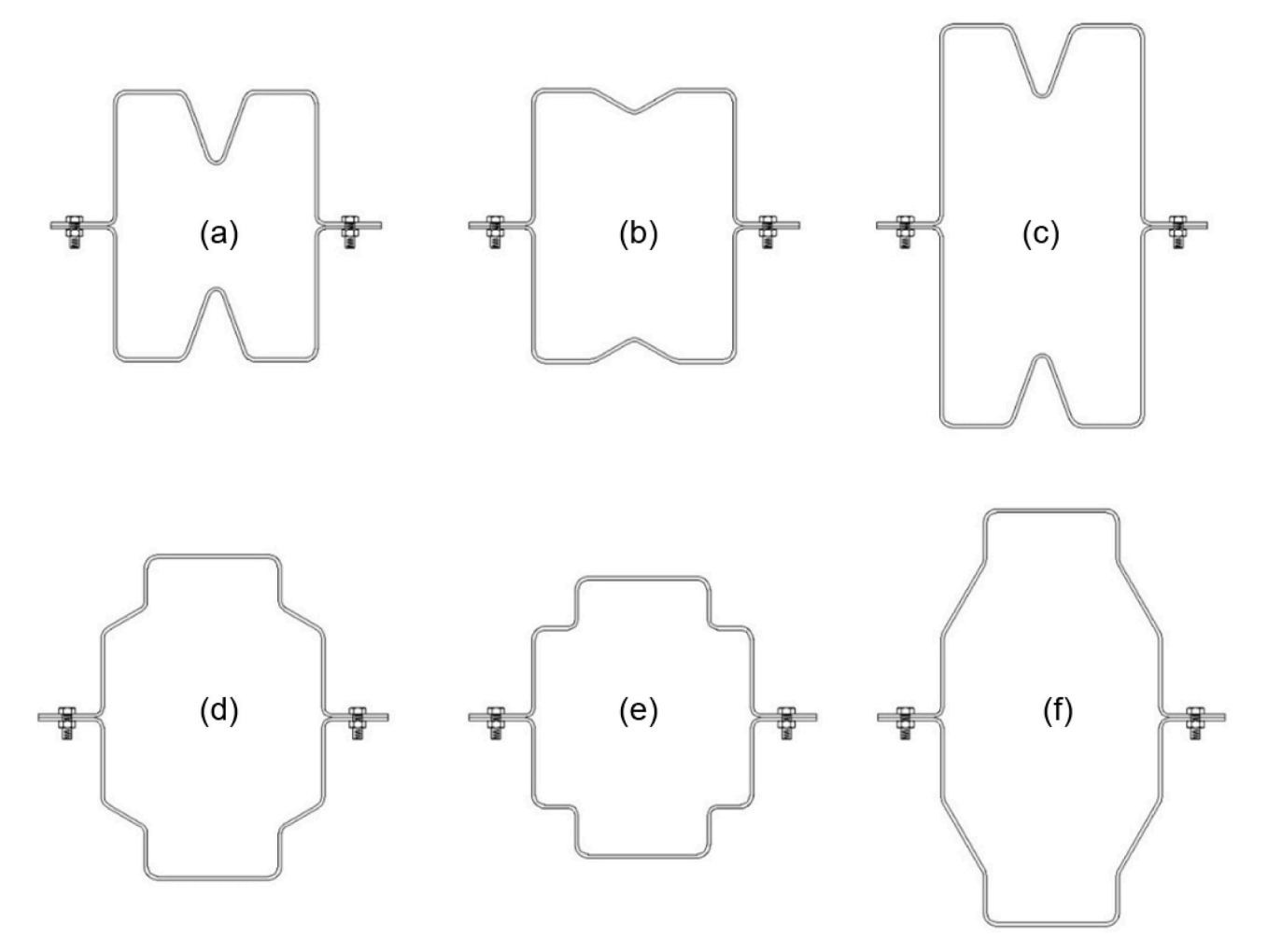


Fig. 9. Built-up closed sections configurations: (a): DM, (b): 15-DM, (c): 17-DM, (d): DOW, (e): 15-DOW, (f): 17-DOW.

$$M_{nl} = \frac{M_y \ for \ \lambda_l \le 0.320}{\left[1 - 0.18 \left(\frac{M_{crl}}{4M_y}\right)^{0.3}\right] \left(\frac{M_{crl}}{4M_y}\right)^{0.3} M_y \ for \ \lambda_l > 0.320}$$
(4)

$$M_{nl} = \frac{\left[1 + (\eta - 1)\left(1 - \frac{1}{C_{yl}^2}\right)M_y\right] \quad for \quad \lambda_l \le 0.949}{\left[1 - 0.03\left(\frac{M_{crl}}{M_y}\right)^{0.3}\right]\left(\frac{M_{crl}}{M_y}\right)^{0.3}M_y \quad for \quad \lambda_l \le 0.949}$$
(5)

For built-up open section named as OV and failed in local buckling the following equation was proposed [30]:

$$M_{nl} = \frac{\left[1 + (\eta - 1)\left(1 - \frac{1}{C_{yl}^2}\right)M_y\right] \quad for \quad \lambda_l \le 0.980}{\left[1 - 0.01\left(\frac{M_{crl}}{M_y}\right)^{0.25}\right]\left(\frac{M_{crl}}{M_y}\right)^{0.25}M_y \quad for \quad \lambda_l \le 0.980}$$
(6)

Additionally, [28] suggested modified DSM equation for double sigma face to face section:

$$M_{nl} = \frac{M_{y} \quad for \quad \lambda_{l} \le 0.5}{\left[1 - 0.2 \left(\frac{M_{crl}}{1.5M_{y}}\right)^{0.33}\right] \left(\frac{M_{crl}}{1.5M_{y}}\right)^{0.33} M_{y} \quad for \quad \lambda_{l} > 0.5}$$
(7)

# 11. Moreover, [32] proposed the following equation for face to face hollow section

$$M_{nl} = \left[1 - 0.15 \left(\frac{M_{crl}}{M_{y}}\right)^{0.25}\right] \left(\frac{M_{crl}}{M_{y}}\right)^{0.25} M_{ne} \quad for \quad \lambda_{l} \le 0.776$$
 (8)

The above proposed equation was obtained by modifying the various constant parameters and adjusting the local slenderness limits. This

equation parameters, it would contradict the current procedure of providing a general DSM equation for built-up sections.

It is important to note that in DSM approach for determining the bending capacity of CFS members, the effect of thickness is indirectly considered through the concept of effective width, which is related to the width-to-thickness ratio (b/t), connecting the basis of DSM to the fundamental EWM. However, the equation for local slenderness  $\lambda_l$ 

 $\sqrt{\frac{M_y}{M_{ct}}}$  prescribed in NAS provisions [34] does not explicitly account for thickness. Considering the significant influence of thickness on the local slenderness of thin-walled members, it is crucial to directly account for thickness when analysing their behavior, particularly in situations where local buckling is likely to prevail. To overcome these challenges while evolving a reliable design method with higher levels of accuracy, a diligent investigation is required to develop a general DSM capable of predicting the flexural strength for different built-up members, or at least, limit the number of design equations for built-up closed and open sections. The fundamental objective of the current study was to establish a unified design approach that can handle the diverse range of non-conventional built-up cross-section that may be encountered in practice.

# 12. Generalized Direct Strength Method for cold-formed steel built-up sections

Based on DSM predictions for DM and DOW sections and the other aspects related to built-up sections, the Generalized Direct Strength Method (DSM-G) has been introduced through suitable judicious adjustments carried out in the original equation as follows:

 For cases where the current DSM underestimates the flexural strengths:

$$M_{DSM-G} = \frac{\eta}{0.1565t^3 - 0.774t^2 + 1.2178t + 0.2732} \left\{ \frac{\left[ M_y + \left( 1 - \frac{1}{C_{yl}^2} \right) (M_p - M_y) \right] \lambda_{lf} \le 0.776}{\left[ 1 - 0.15 \left( \frac{M_{crl}}{M_y} \right)^{0.4} \right] \left( \frac{M_{crl}}{M_y} \right)^{0.4} M_y \quad \lambda_{lf} > 0.776} \right\}$$

$$(9)$$

modification has a significant impact on the inelastic reserve for the concerned section since the current slenderness limit ( $\lambda_l \leq 0.776$ ) may not adequately reflect the actual slenderness values obtained from the slenderness curves. Additionally, considering a single local slenderness

 For cases where the current DSM overestimates the flexural strengths:

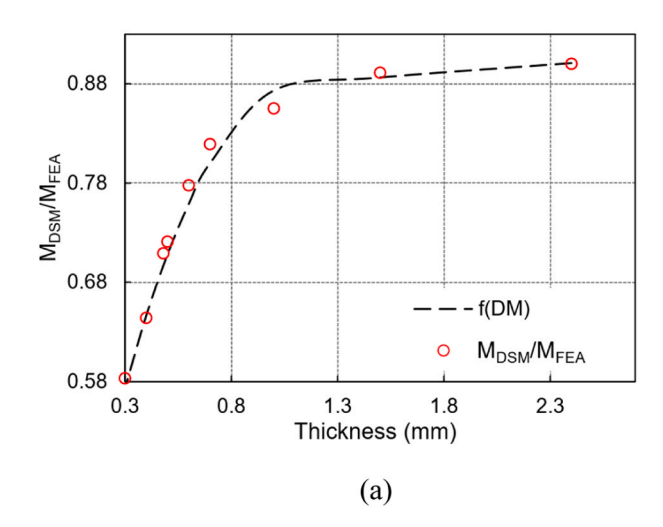
$$M_{DSM-G} = \eta \cdot (0.1565t^3 - 0.774t^2 + 1.2178t + 0.2732) \left\{ \frac{\left[M_y + \left(1 - \frac{1}{C_{yf}^3}\right) (M_p - M_y)\right] \lambda_{lf} \le 0.776}{\left[1 - 0.15 \left(\frac{M_{crl}}{M_y}\right)^{0.4}\right] \left(\frac{M_{crl}}{M_y}\right)^{0.4} M_y \quad \lambda_{lf} > 0.776} \right\}$$

$$(10)$$

limit, regardless of the section shape, by analysing data sets from single-element profiles, may not account for the behavioural variations resulting from different assembling methods and approaches used for built-up sections. However, if we were to follow the previous suggestions and treat the uniqueness of slenderness individually for each section, by adopting a new modified local slenderness limit and constant

Eq. (9) and (10) were developed based on the following hypothesis, both of which represent observed limitations when applying the current DSM equation to built-up sections:

 Ultra-thin sections often demonstrate distinct failure modes and behaviour compared to thicker sections. They are more prone to



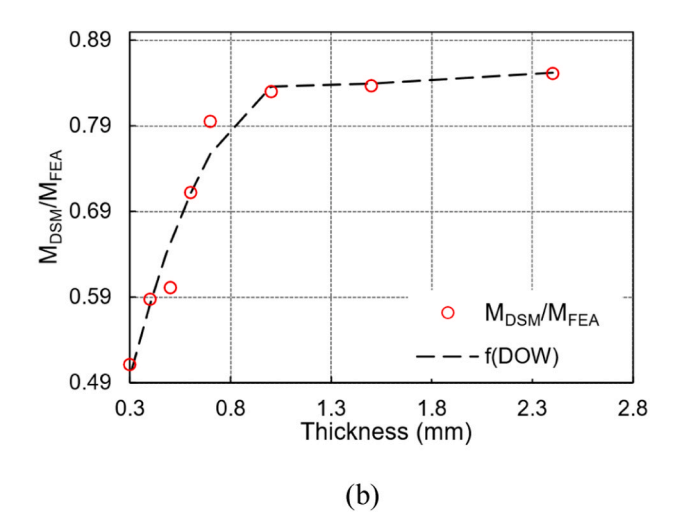


Fig. 10. Polynomial distribution of M<sub>DSM</sub>/M<sub>FEA</sub> ratio with respect to thickness for: a) DM sections, b) DOW sections.

Table 10 Metrics and Coefficients of Shape  $\eta$  determination.

		1	
t (mm)	$M_{DSM}/M_{FEA}$ (DM)	$M_{DSM}/M_{FEA}$ (DOW)	$\eta = f_{DM}(t)/f_{DOW}(t)$
2.40	0.901136	0.851968	1.06
1.50	0.8865875	0.839350	1.06
1.00	0.8735	0.836400	1.04
0.70	0.8000795	0.757278	1.06
0.60	0.759044	0.711064	1.07
0.50	0.7081625	0.653000	1.08
0.48	_	0.639863	_
0.40	0.646496	0.581928	1.11
0.30	0.5731055	0.496690	1.15
Mean	_	_	1.08
COV	_	_	0.032
R <sup>2</sup> (COD)	72%	59%	_
MSPE	0.000168	0.00156	_

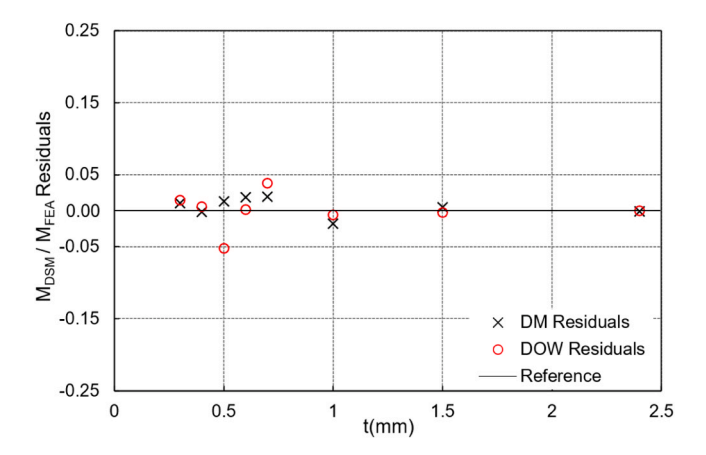


Fig. 11. Residual analysis for prediction model of DM and DOW sections.

local buckling, distortional buckling, and other instability phenomena. The current DSM equations were primarily derived from test data of thicker sections and fails to capture these unique characteristics fully. Therefore, it may not be suitable for thinner sections.

• The adoption of fictive slenderness  $\lambda_{lf} \leq 0.776$ , which may not reflect the actual slenderness of the built-up sections, as discussed before. Nevertheless, after the modified flexural strength  $M_{DSM-G}$  is calculated, the actual slenderness and inelastic reserve of the sections will be determined using slenderness curves. Indeed, this strategy prevents changes to the current equation and provides a robust way

to dealing with built-up sections. This approach avoids alterations in the current equation, and brings a solid approach to treat built-up sections.

# 13. Development of DSM-G equations (Regression analysis and shape coefficient)

While developing the DSM-G equations, a nonlinear regression analysis was performed to establish a relationship between the dependent variable  $\frac{M_{DSM}}{M_{PEA}}$ , and the independent variable represented by the sectional thickness to find the accurate function describing the relationship between the two, and these on multiple cross sectional configurations of DM and DOW sections as presented in Fig. 9. The regression analysis produced a meaningful pattern indicating that adjustments in thickness had a pronounced impact on the conservativeness level. With a reduction in the cross-sectional thickness, the deviation from the accurate solution amplified, leading to  $M_{FEA}M_{DSM}$  significantly exceeding unity. Based on this pattern, curves presented in Fig. 10 (a&b), illustrate the variation of  $M_{DSM}M_{FEA}$  ratio with regards to the thickness variation for both DM and DOW sections. Given the similarity in shape between the two curves, this variation could be presented by cubic equations, which proved

$$\frac{M_{DSM}}{M_{FEA}} = f_{DM}(t) = 0.1565t^3 - 0.774t^2 + 1.2178t + 0.2732For \quad DM \quad section \tag{11}$$

$$\frac{M_{DSM}}{M_{FEA}} = f_{DOW}(t)$$

$$= 0.193t^3 - 0.9399t^2 + 1.4389t + 0.1444For \quad DOW \quad section$$
 (12)

to be a good fit to the data set points, as presented in the following mathematical model:

To verify the mathematical model's ability in predicting the variations in the relationship between the variables, the coefficient of determination ( $\rm R^2$ ) was calculated. It was found that the model effectively explains 72% of this variability within DOW section, and 59% within DM section as shown in Table 10. The Mean Square Prediction Error (MSPE) coefficient results were 0.00156 for DOW section and 0.000168 for DM section, which highlights the good alignment between the predictive model and the data points. Furthermore, the adequacy of the model was assessed by conducting a residual analysis. The outcomes of this analysis are presented in Fig. 11, offering a visual interpretation to the model's capacity to capture the relationship between the thickness and the  $\rm M_{DSM}/M_{FEA}$  ratio. In a nutshell, these values can be classified as ranging from acceptable to good. Given the innovative nature of

Table 11
Comparison of predicted strengths (DSM vs. DSM-G) for DM sections.

S. No	Specimen	M <sub>FEA</sub> (kN.mm)	M <sub>DSM</sub> (kN.mm)	M <sub>DSM-G</sub> (kN.mm)	$ m M_{FEA}/ m M_{DSM}$	$M_{FEA}/M_{DSM-G}$
1	DM-2.4	12434	11355	12601	1.10	0.99
2	DM-1.5	7517	6681	7536	1.13	1.00
3	DM-1.0	4881	4202	4811	1.16	1.01
4	DM-0.7	3094	2631	3288	1.18	0.94
5	DM-0.6	2452	2050	2701	1.20	0.91
6	DM-0.5	1935	1524	2152	1.27	0.90
7	DM-0.48	1904	1398	2007	1.36	0.95
8	DM-0.4	1544	1061	1641	1.46	0.94
9	DM-0.3	977	651	1136	1.50	0.86
10	15-DM- 2.4	11101	10049	11151	1.10	1.00
11	15-DM- 1.5	6688	6145	6931	1.09	0.96
12	15-DM- 1.0	4282	3913	4480	1.09	0.96
13	15-DM- 0.7	2805	2427	3033	1.16	0.92
14	15-DM- 0.6	2248	1882	2479	1.19	0.91
15	15-DM- 0.5	1759	1409	1990	1.25	0.88
16	15-DM-	1740	1317	1890	1.32	0.92
17	0.48 15-DM-	1491	973	1505	1.53	0.99
18	0.4 15-DM-	1203	602	1050	2.00	1.15
19	0.30 17-DM-	22230	19621	21774	1.13	1.02
20	2.4 17-DM-	13296	11515	12988	1.15	1.02
21	1.5 17-DM-	8253	6533	7479	1.26	1.10
22	1.0 17-DM-	4903	3643	4553	1.35	1.08
23	0.7 17-DM-	4259	2810	3702	1.52	1.15
24	0.6 17-DM-	3577	2054	2900	1.74	1.23
25	0.5 17-DM-	3017	1922	2758	1.57	1.09
26	0.48 17-DM-	2379	1412	2184	1.68	1.09
27	0.4 17-DM-	2250	1288	2035	1.75	1.11
	0.38 bility index $\beta_1$ bility index $\beta_2$				1.34 0.18 3.58 3.75	1.00 0.094 3.04 3.24

this approach, devoid of any pre-existing benchmarks, these results will serve as a valuable reference for future studies.

To take an account the influence of cross-sectional shape on the bending capacity, a proportionality coefficient was defined between the two curves based on the data set reported in Table 10. Due to its dependence on section shape, this coefficient also known as shape coefficient features the relationship between the two curves. In case of DM sectional configurations, the shape coefficient will take a value of 1, since Eq. (9) and (10) are based on DM sectional results. However, for DOW sectional configurations a mean value of 1.08 from the ratio of  $\frac{f_{DM}(t)}{f_{DOW}(t)}$  at each point, is presented in Table 10 with a coefficient of variation (COV) = 3.27%, indicating that the values are well gathered around the mean. It is important to note that this coefficient could be different depending on the lead equation. Indeed, notable differences could be observed if the (DSM-G) equations will be based on Eq. (12) instead of (11), and may impact the flexural strength prediction. However, the outcome will be the same in terms of precision and application of the proposed equations. The proposition of a shape coefficient was carried out mainly to substantiate the claim that built-up sections have

Table 12
Comparison of predicted strengths (DSM vs. DSM-G) for DOW sections.

S. No	Specimen	M <sub>FEA</sub> (kN.mm)	M <sub>DSM</sub> (kN.mm)	M <sub>DSM-G</sub> (kN.mm)	$M_{FEA}/M_{DSM}$	$M_{FEA}/M_{DSM-G}$
1	DOW-2.4	12662	11094	13296	1.14	0.95
2	DOW-1.5	7697	6525	8096	1.18	0.95
3	DOW-1.0	4791	3818	4808	1.25	1.00
4	DOW-0.7	2565	2138	2939	1.20	0.87
5	DOW-0.6	2281	1646	2385	1.39	0.96
6	DOW-0.5	1995	1219	1893	1.64	1.05
7	DOW-0.48	2094	1135	1791	1.85	1.17
8	DOW-0.4	1312	840	1429	1.56	0.92
9	DOW-0.3	1046	511	982	2.05	1.07
10	15-DOW- 2.4	10596	8526	10408	1.24	1.02
11	15-DOW- 1.5	6425	5260	6526	1.22	0.98
12	15-DOW- 1.0	4053	3311	4170	1.22	0.97
13	15-DOW- 0.7	2242	1643	2259	1.36	0.99
14	15-DOW- 0.6	1898	1247	1807	1.52	1.05
15	15-DOW- 0.5	1522	871	1353	1.75	1.12
16	15-DOW- 0.4	1263	767	1305	1.65	0.97
17	15-DOW- 0.3	948	506	971	1.87	0.98
18	17-DOW- 2.4	17667	15439	18846	1.14	0.94
19	17-DOW- 1.5	10666	9008	11176	1.18	0.95
20	17-DOW- 1.0	5997	5264	6629	1.14	0.90
21	17-DOW- 0.7	3595	2949	4054	1.22	0.89
22	17-DOW- 0.6	3001	2276	3298	1.32	0.91
23	17-DOW- 0.5	2730	1690	2625	1.62	1.04
24	17-DOW- 0.4	2238	1152	1960	1.94	1.14
25	17-DOW- 0.38	1649	1059	1841	1.56	0.90
Mean					1.45	0.99
COV					0.32	0.080
Reliab	ility index β <sub>1</sub>		3.42	2.66		
Reliab	ility index β <sub>2</sub>				3.58	2.86

approximately the same polynomial distribution in terms of thickness variation. Hence, it is possible to determine this coefficient through trial and error to obtain the convenient coefficient for the investigated built-up section.

It is important to note that Eq. (10), unlike Eq. (9), did not undergo regression analysis. This omission is attributed to its dependence on the initial hypothesis assumption, asserting that all built-up sections facing failure strength prediction in the original DSM equation will exhibit the same strength variation when altering the thickness. As a result, conducting an additional regression analysis was deemed unnecessary.

### 14. DSM-G prediction for DM and DOW

In the process of validating the proposed method, a comprehensive validation on 52 beams (both DM and DOW sections) is conducted to assess the accuracy of the new method in predicting their flexural strengths. Tables 11 and 12 show the flexural strengths of  $M_{DSM-G}$  for DM and DOW sections respectively. Remarkably, an accurate flexural strength prediction has been recorded for both the sectional profiles, with a mean value ( $M_{FEA}M_{DSM-G}$ ) of 1.00 for DM sections and 0.99 for DOW sections. The coefficient of variation (COV) of 9.4% for DM and 8.0% for DOW was obtained, indicating a low variation degree in results. Moreover, the reliability of the new design is assessed with reliability

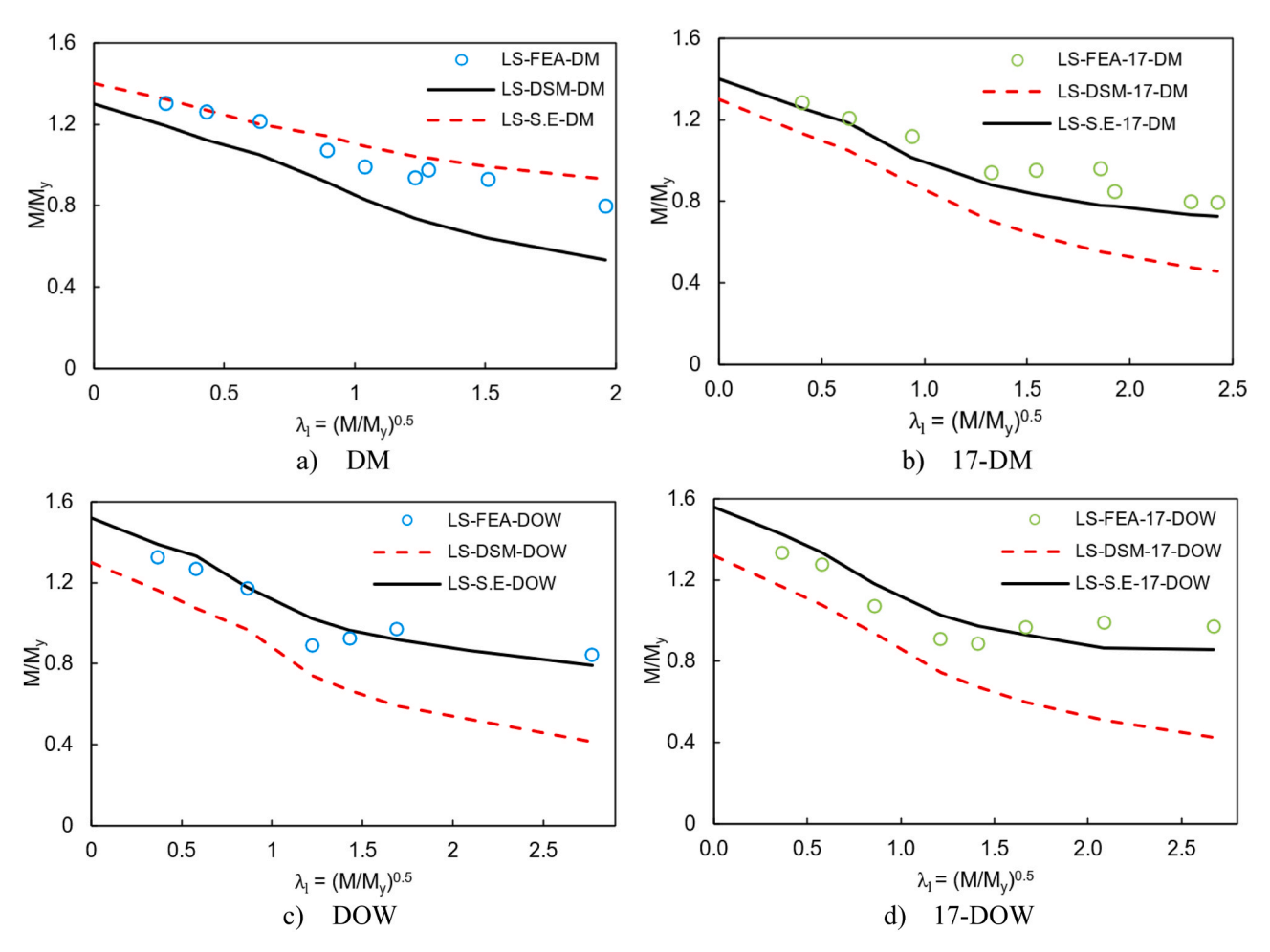


Fig. 12. Local buckling design curves for: a) DM, b) 17-DM, c) DOW, d) 17-DOW.

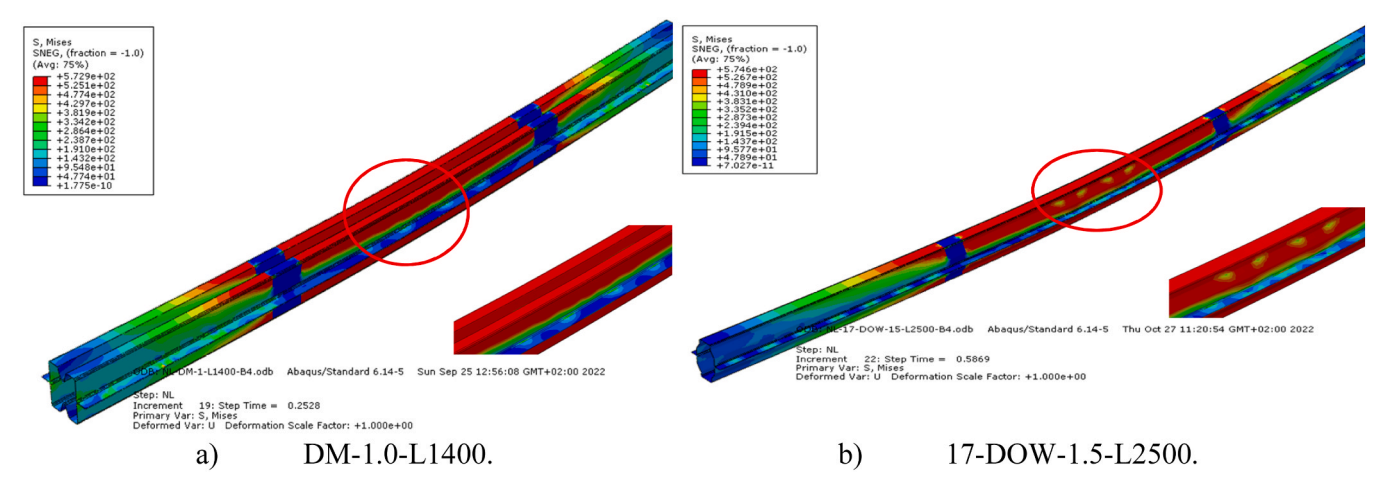


Fig. 13. Local buckling failure limits for: a) DM-1.0-L1400, b) 17-DOW-1.5-L2500 specimens.

index  $\beta_1$  and  $\beta_2$  calculation, surpassing the target reliability value  $\beta_0 = 2.5$ , assuring a higher reliability of the new design equation.

### 15. Local buckling design curves

Fig. 12 presents local buckling design curves for sections DM and DOW, with local slenderness curves provided for both design (DSM, DSM-G) and FEA strengths for each sectional configuration. The distribution of  $M/M_{\gamma}$  was plotted by varying the local slenderness ratio ( $\lambda_l$ )

across a wide range of thicknesses [0.3–2.4]. The limits of the local slenderness ratio were determined graphically, where the curve's shape transitions from linearity to a sudden drop in the flexural strength  $\frac{M}{M_{\rm y}}$ . For 17-DOW section, local buckling failure of specimens starts at  $\lambda_l=0.580$ , corresponding to t = 1.5 mm, as shown in Fig. 12(d), and its deformed shape is shown in Fig. 13(b). In case of DM section, local buckling occurred at  $\lambda_l=0.636$  corresponding to t = 1 mm. Fig. 13(a), demonstrates the lower impact of local buckling (LB) on the overall strength of

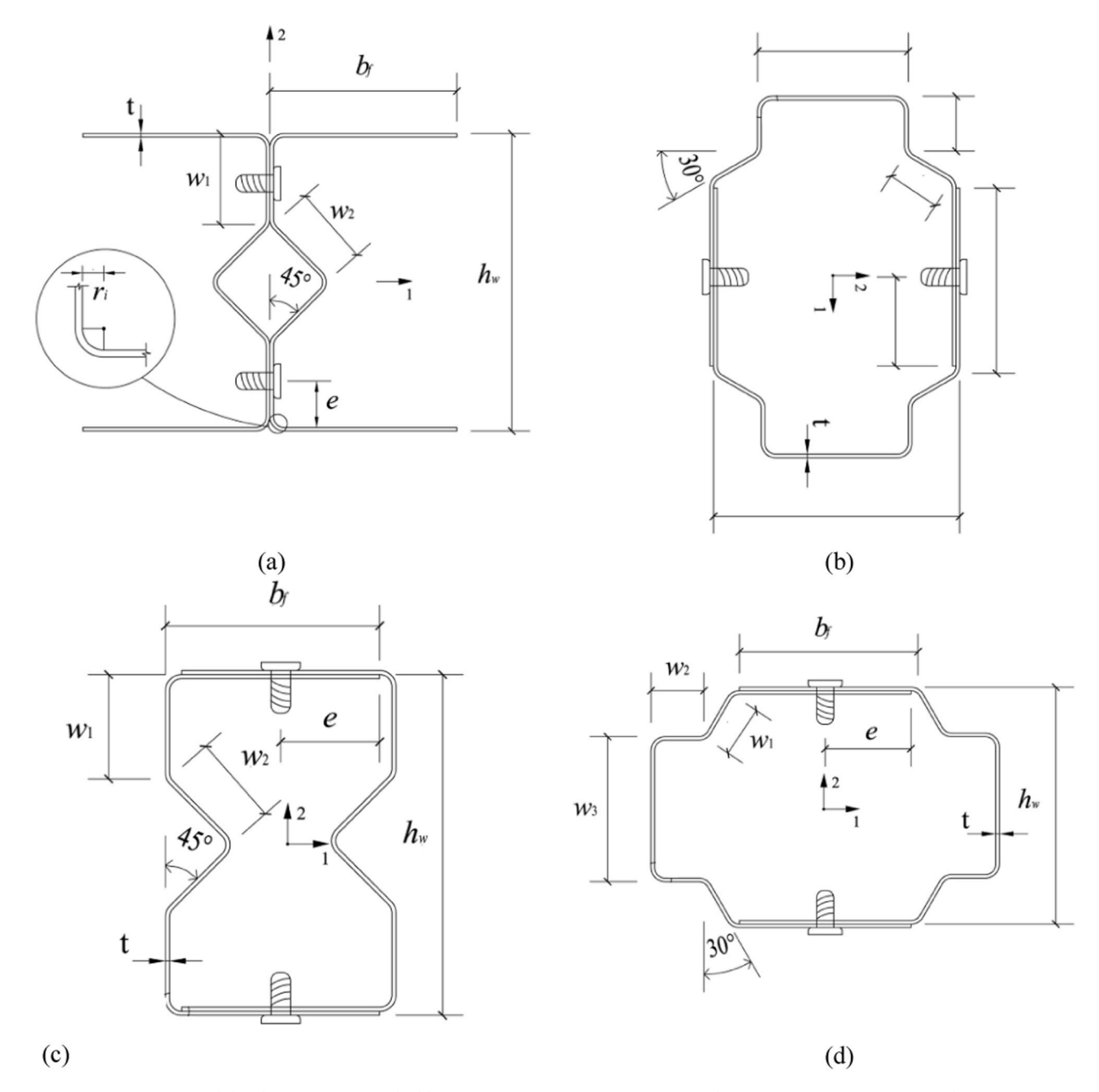


Fig. 14. Cross-sectional details of specimens studied by Wang & Young [29]: (a) OV section; (b) COW section; (c) CV section; (d) COF section.

DM section, which aligns with the slenderness curves (see Fig. 12(a)), indicating its superior behaviour in preventing local buckling among all the investigated configurations.

In general, LC-G slenderness curves align well with FEA strengths compared to LC-DSM curves. The local slenderness limit at which the sections fail in local buckling corresponds to  $\frac{M_{DSM}-g}{M_y}>1$  instead of  $\frac{M_{DSM}}{M_y}=1$ , This discrepancy is due to major changes made to the original DSM Eq. (1). This slenderness threshold ensures that the element remains within a safe range of slenderness to avoid local buckling failure.

### 16. Validating DSM-G against other Built-up sections [29,30]

The fundamental goal behind developing a DSM-G for built-up sections was to avoid its application to the sections studied in the current investigation. This demands a robust approach encompassing a wide range of built-up sections. In this context, the built-up open and closed

sections extracted from the tests and parametric studies as reported in [29,30] were used for this verification, chosen over a wide variational range of dimensional parameters altered. This renders it convenient for validating the proposed method. Like the DM and DOW sections, the nomenclature of OV, COW, CV and COF sections followed the same reasoning. "OV" denotes an open double sigma section, forming a rounded 'O' shape with a 'V' shape stiffener in the middle (see Fig. 14(a)). "COW" represents a closed section 'C' resulting in an overall round shape resembling letter 'O' with 'W' shaped stiffeners (see Fig. 14(b)). "CV" refers to a closed double sigma section (C) with middle stiffeners forming a 'V' shape (see Fig. 14(c)). "COF" is the reversed version of the COW section (see Fig. 14(d)). Tables 13-15 present the predicted flexural strength  $(M_{DSM-G})$  compared to the maximum bending moment obtained from finite element analysis ( $M_{FEA}$ ), on a total of 71 beams. Also, the predicted flexural strengths using the proposed equations by Wang & Young (MDSM-W&Y) were also presented. The mean values of

Table 13
Comparison of predicted strengths (DSM vs. DSMW&Y vs. DSM-G) for OV sections.

Specimen	$M_{Test}$	$M_{DSM}$	$M_{DSM\text{-}}$	$M_{DSM\text{-}}$	$M_{Test}$	$M_{Test}$	$M_{Test}$
	or		W&Y	G	$M_{DSM}$	$M_{DSM}$	$M_{DSM}$
	$M_{FEA}$				or	W&Y	G
	(kN.				$M_{FEA}$	or	or
	mm)				$M_{DSM}$	$M_{FEA}/$	$M_{FEA}/$
						$M_{DSM}$	$M_{DSM-}$
						W&Y	G
12-OV-	13844	12961	11446	17205	1.07	1.21	0.80
1.9							
13-OV-	13183	12797	11397	16988	1.03	1.16	0.78
1.9							
12-OV-	11271	8784	10315	11394	1.28	1.09	0.99
1.5							
13-OV-	10465	8670	10189	11246	1.21	1.03	0.93
1.5	10000	0064	10050	11100	1.00	0.00	0.00
2-OV-1.9	10290	8364	10352	11103	1.23	0.99	0.93
1-OV-1.9	9988	8318	10314	11042	1.2	0.97	0.90
9-OV-1.9	16971	13138	16313	17440	1.29	1.04	0.97
5-OV-1.9	22756	17544	21807	23289	1.3	1.04	0.98
10-OV- 1.9	16480	12989	16152	17242	1.27	1.02	0.96
1.9 12-OV-	7128	4439	5631	5844	1.61	1.27	1.22
1.0	/120	4439	3031	3044	1.01	1.2/	1.22
13-OV-	5271	4382	5565	5769	1.2	0.95	0.91
1.0	02/1	1002	0000	0,03	1.2	0.50	0.71
2-OV-1.5	6985	5596	7275	7259	1.25	0.96	0.96
1-OV-1.5	7584	5563	7248	7216	1.36	1.05	1.05
5-OV-1.5	16431	11719	15314	15201	1.4	1.07	1.08
7-OV-1.5	15346	11580	15153	15021	1.33	1.01	1.02
2-OV-1.0	4031	2781	3970	3661	1.45	1.02	1.10
9-OV-1.0	6571	4356	6249	5735	1.51	1.05	1.15
5-OV-1.0	8549	5814	8350	7654	1.47	1.02	1.12
10-OV-	5952	4308	6189	5672	1.38	0.96	1.05
1.0							
7-OV-1.0	7828	5743	8262	7561	1.36	0.95	1.04
9-OV-0.6	2861	1781	2909	2698	1.61	0.98	1.06
10-OV-	2639	1762	2883	2670	1.5	0.92	0.99
0.6							
7-OV-0.6	3614	2350	3851	3560	1.54	0.94	1.02
OV-0.48-	1246	774	1378	1278	1.61	0.9	0.98
B4	4000	0011	4051	0701	1.51	1.05	1.15
OV-1.0-	4238	2811	4051	3701	1.51	1.05	1.15
B4					1.06	1.00	1.00
Mean (P <sub>m</sub> )					1.36	1.03	1.00
COV	4 ^				0.123	0.083	0.101
Reliability i			3.87	3.00	2.85		
Reliability i	ınαex $β_2$	4.06	3.84	3.74			

 $M_{EXP~or~FEA}/M_{DSM-G}$  for the OV, COW, CV and COF sections and their different configurations were 1.00, 0.99, 1.02 respectively, with a COV of 10.1%, 9.8% and 7.8%. This is considered as a low degree of variation, indicating that the strength of the specimens is well gathered around the mean values. The reliability of the proposed design approach was verified by calculating the reliability index ( $\beta_1$ ) and ( $\beta_2$ ), which was found to surpass the target reliability 2.5 as prescribed in NAS [34].

The flexural strength values obtained from finite element analysis ( $M_{Test}$  /  $_{FEA}$ ) align accurately with those predicted by the generalised DSM ( $M_{DSM-G}$ ), whether in over-conservative cases as for OV and COW sections, where the strength is predicted using Eq. (9), or unconservative cases represented by CV and COF sections using Eq. (10). The shape coefficients used for these sections as well as for the sections investigated in this study (DM and DOW) are presented in Fig. 15. This results highlights the accuracy and reliability of the design approach, for providing accurate estimates for the strength of built-up sections susceptible to local buckling failure.

### 17. Conditions to be satisfied for adopting DSM-G

Before applying the proposed equations presented in this study, two conditions must be fulfilled:

Table 14
Comparison of predicted strengths (DSM vs. DSMW&Y vs. DSM-G) for COW sections

Specimen	M <sub>FEA</sub> (kN mm)	M <sub>DSM</sub> (kN mm)	M <sub>DSM</sub> - w&Y (kN mm)	M <sub>DSM</sub> - <sup>G</sup> (kN mm)	$\begin{array}{c} M_{Test}/\\ M_{DSM}\\ or\\ M_{FEA}/\\ M_{DSM} \end{array}$	M <sub>Test</sub> / M <sub>DSM</sub> - w&Y or M <sub>FEA</sub> / M <sub>DSM</sub> - w&Y	$M_{Test}/M_{DSM}$ $G$ $Or$ $M_{FEA}/M_{DSM}$ $G$
15-COW-	11635	9242	11434	10769	1.26	1.02	1.08
2.4 14-COW- 2.4	14185	11161	13798	13005	1.27	1.03	1.09
17-COW- 2.4	19024	15835	19568	18451	1.20	0.97	1.03
19-COW- 1.9	19407	16014	19354	19409	1.21	1.00	1.00
21-COW- 2.4	16856	13468	15950	15693	1.25	1.06	1.07
15-COW- 1.5	7002	5491	6446	6503	1.28	1.09	1.08
1.5 14-COW- 1.5	8407	6628	7769	7850	1.27	1.08	1.07
17-COW- 1.5	11232	9398	11007	11130	1.20	1.02	1.01
15-COW- 1.0	4508	3259	3682	3918	1.38	1.22	1.15
19-COW- 1.0	7674	7282	8229	8753	1.05	0.93	0.88
21-COW- 2.4	16856	13468	15950	15693	1.25	1.06	1.07
17-COW- 1.0	6745	5543	6268	6663	1.22	1.08	1.01
22-COW- 2.4	19151	16554	19016	19289	1.16	1.01	0.99
22-COW- 1.5	10410	7501	9062	8884	1.39	1.15	1.17
COW- 0.48- B4	1699	1418	1735	2137	1.20	0.98	0.80
COW-1.0- B4	4691	4321	4888	5194	1.09	0.96	0.90
COW-1.0- B4R	4730	4321	4888	5194	1.09	0.97	0.91
Mean (P <sub>m</sub> ) COV (V <sub>P</sub> ) Reliability i Reliability i					1.22 0.072 3.87 4.06	1.04 0.067 3.00 3.84	1.02 0.098 2.85 3.74

- 1. Elastic buckling failures of built-up sections must be carefully investigated. Some sections may fail with an interaction between multiple modes such as (LB & DB) or (LB & LTB). The nominal buckling load may also be recorded for failure modes other than local buckling. Numerous other parameters may affect the nominal buckling moment, such as the span, support conditions, thickness, and geometrical properties. In situations where these conditions prevail, the application of the generalised equations need to be assessed before extending it.
- In the current investigation, the thickness was limited to 2.4 mm. For greater thickness values, more investigations need to be carried out to check the adequacy in that range.

### 18. Guidelines for using DSM-G

Fig. 16 presents the flow chart to be followed while using DSM-G. To effectively use DSM-G (Eq.s (9)&(10)) for predicting the flexural strength of novel unconventional built-up sections, the following steps are recommended:

• Determine the flexural strength based on the original DSM using the nominal local buckling moment  $M_{nl}$  (Eq. (1)), considering  $\lambda_l$  as a fictive local slenderness limit  $\lambda_{lf} \leq 0.776$ .

Table 15
Comparison of predicted strengths (DSM vs. DSMW&Y vs. DSM-G) for CV and COF sections.

Specimens	$M_{EXP}$ or $M_{FEA}$ (kN mm)	M <sub>DSM</sub> (kN mm)	M <sub>DSM-W&amp;Y</sub> (kN mm)	M <sub>DSM-G</sub> (kN mm)	$M_{EXP}/M_{DSM}$ or $M_{FEA}/M_{DSM}$	$\begin{array}{l} M_{EXP}/M_{DSM\text{-}W\&Y} \\ or \ M_{FEA}/M_{DSM\text{-}W\&Y} \end{array}$	$\rm M_{EXP}/\rm M_{DSM\text{-}G}$ or $\rm M_{FEA}/\rm M_{DSM\text{-}G}$
6-CV-2.4	30827	34929	29554	27069	0.88	1.04	1.14
1-CV-1.9	9939	12924	10784	9629	0.77	0.92	1.03
4-CV-1.9	9840	12649	10485	9424	0.78	0.94	1.04
10-CV-1.9	16629	20150	15904	15012	0.83	1.05	1.11
1-CV-1.5	7145	9975	7711	7606	0.72	0.93	0.94
4-CV-1.5	7300	9759	7496	7441	0.75	0.97	0.98
6-CV-1.5	15638	20736	14994	15810	0.75	1.04	0.99
3-CV-1.0	3867	6216	4233	4670	0.62	0.91	0.83
7-CV-1.5	15343	20067	13640	15300	0.76	1.12	1.00
4-CV-1.0	3805	6138	4139	4611	0.62	0.92	0.83
10-CV-1.0	7482	9222	6178	6928	0.81	1.21	1.08
6-CV-1.0	8179	12251	8228	9203	0.67	0.99	0.89
7-CV-1.0	7609	10748	7415	8074	0.71	1.03	0.94
10-CV-0.6	2872	3968	2858	2590	0.72	1.01	1.11
7-CV-0.6	3807	4555	3403	2973	0.84	1.12	1.28
CV-0.48-B4	1266	2018	1501	1209	0.63	0.84	1.05
CV-1.0-B4	4088	6734	4460	5059	0.61	0.92	0.81
22-COF-2.4	31949	36259	29527	28100	0.88	1.08	1.14
14-COF-1.5	6216	7969	6284	6076	0.78	0.99	1.02
19-COF-1.9	9992	15630	11048	11645	0.64	0.9	0.86
15-COF-1.0	2934	4766	3352	3580	0.62	0.88	0.82
21-COF-1.0	5118	7100	4940	5334	0.72	1.04	0.96
17-COF-1.0	3582	5685	3906	4271	0.63	0.92	0.84
22-COF-1.0	9883	11967	8156	8990	0.83	1.21	1.10
21-COF-0.6	2542	3336	2308	2178	0.76	1.1	1.17
19-COF-1.0	3611	6150	4291	4620	0.59	0.84	0.78
COF-0.48-B4	1278	1915	1397	1147	0.67	0.91	1.11
COF-1.0-B4	3749	5523	3792	4149	0.68	0.99	0.90
COF-1.0-B4R	3884	5523	3792	4149	0.7	1.02	0.94
Mean(P <sub>m</sub> )					0.73	1.00	0.99
$COV(V_p)$					0.113	0.094	0.129
Reliability inde	$ex \beta_1$				1.55	2.80	2.94
Reliability inde	ex β <sub>2</sub>				1.74	3.00	3.14

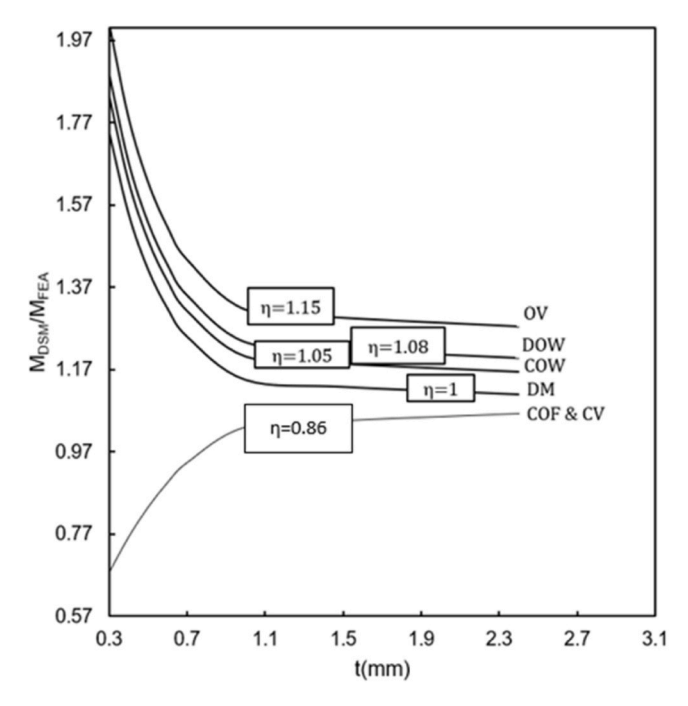


Fig. 15. Sections distribution curves for different form coefficient  $\eta$ .

• Calculate the flexural strength ratio  $M_{FEA}/M_{DSM}$ . If the DSM equation underestimates the flexural capacity of the built-up section, i.e.,  $M_{FEA}/M_{DSM} > 1.00$ , use the following equation:

$$M_{DSM-G} = \frac{\eta}{0.1565t^3 - 0.774t^2 + 1.2178t + 0.2732} M_{nl}$$
 (9)

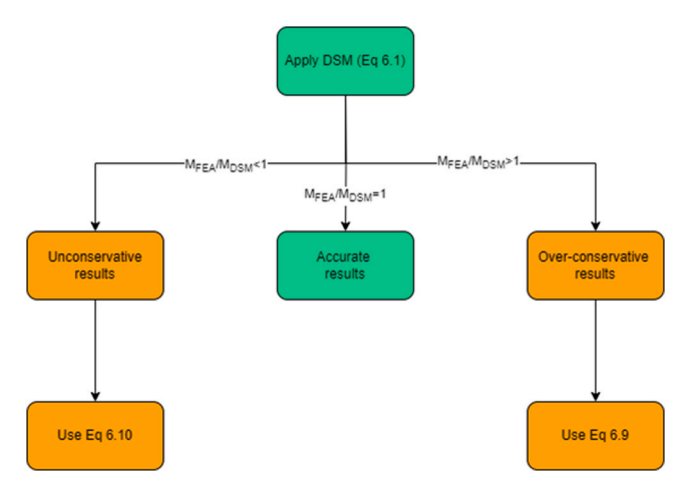


Fig. 16. Flowchart to be followed while adopting DSM-G.

Conversely, If the DSM equation overestimates the flexural capacity of the built-up section, i.e.,  $M_{FEA}/M_{DSM} < 1.00$ , use the following equation:

$$M_{DSM-G} = \eta. (0.1565t^3 - 0.774t^2 + 1.2178t + 0.2732).M_{nl}$$
 (10)

ullet Determine the shape coefficient  $\eta$  through iterative trials and errors, considering at least three sectional configurations for the built-up section. This ensures a comprehensive coverage of geometrical variations.

Based on the findings of the current study involving DM, DOW, OV, COW, CV, and COF built-up sections, it was observed that Eq. 9 is well-suited for DM, DOW, OV, and COW built-up sections, while Eq. 10 is more appropriate for CV and COF built-up sections.

The values of the correspondent shape coefficient for each section are presented in Fig. 15.

#### 19. Conclusion

This work presents a new approach to the design of built-up sections, developed through a comprehensive numerical investigation of two innovative closed sections. First, a FE model was developed and validated against suitable test results extracted from literature. The validated model was used to study the influence of screw spacing on the flexural strength and deformed shapes of two innovative sections (DM & DOW). This analysis aimed to assess the appropriateness of the double thickness assumption in predicting the design flexural strengths. Furthermore, the elastic buckling behaviour of the sections was analysed using signature curves generated by CUFSM software. The development of the new equations followed by carrying out a parametric study by varying geometrical parameters and focusing local buckling governed cases. This study revealed that the current DSM equations used for predicting the bending strength underestimate the flexural capacity of the beams, resulting in highly conservative results. Moreover, the degree of conservativeness was high, particularly for ultra-thin specimens. This pattern was rigorously examined through the results of the present investigation and previous studies conducted on thin-walled sections. Therefore, regression analysis was conducted to contribute to developing a mathematical model used in the generalised equations for builtup sections. It is important to highlight that the developed equations rely on the conservativeness concept rather than the local slenderness limit ratio ( $\lambda_l$ ), as in the original DSM equation. Two separate equations were introduced to address both over-conservative and unconservative cases. By applying the generalised equation to built-up sections, the following conclusion could be highlighted:

- The proposed equation M<sub>DSM-G</sub>, could accurately predict the flexural strength of built-up closed and open sections susceptible to failure by local buckling.
- DSM-G is accurate in predicting the strengths of ultra-thin sections.
- Unification of modified DSM equations for built-up sections through the concept of conservativeness instead of local slenderness ratio limits.
- Estimation enhancement of local buckling strength for sections DM and DOW by considering post-yield buckling failure, where  $\frac{M}{M_y} > 1$  corresponds to slenderness limits ratios, which found to be in good agreement with FEA results.
- The screws spacing did not affect local buckling strength of DM and DOW sections, however a minimum spacing is required to avoid distortional deformation thought separation of the individual cross sections.

### CRediT authorship contribution statement

Yazid Hadidane: Writing – review & editing, Supervision, Formal analysis. Salah-Eddine Maizi: Writing – review & editing, Writing – original draft, Validation, Software, Methodology, Investigation, Formal analysis, Data curation, Conceptualization. Mohammad Adil Dar: Writing – review & editing, Writing – original draft, Validation, Formal analysis.

### **Declaration of Competing Interest**

The authors declared no potential conflicts of interest with respect to the research, authorship, and/or publication of this article.

### **Data Availability**

Data will be made available on request.

### Appendix-I

This appendix details two examples for determining the flexural design strengths of the novel built-up sections presented in this study using DSM-G.

- (a) Specimen DM-1.5 and
- (b) Specimen CV-0.48
- (a) For specimen DM-1.5, the material properties E=216 GPa and  $\sigma_{0.2}=572$  MPa. For DM section, we have to use Eq. 9 replicated below:

$$M_{DSM-G} = \frac{\eta}{0.1565t^3 - 0.774t^2 + 1.2178t + 0.2732} M_{nl}$$
(11)

where, 
$$M_{nl} = \begin{cases} M_{y} + \left(1 - \frac{1}{C_{yl}^{2}}\right) (M_{p} - M_{y}) & for \quad \lambda_{lf} \leq 0.776 \\ \left[1 - 0.15 \left(\frac{M_{crl}}{M_{y}}\right)^{0.4}\right] \left(\frac{M_{crl}}{M_{y}}\right)^{0.4} M_{y} & for \quad \lambda_{lf} > 0.776 \end{cases}$$
 (12)

The terms  $M_{crl}$  and  $M_p$  shall be determined in accordance with the guidelines provided in section F2.4.2 of NAS [34], and  $\lambda_{lf}$  is the fictive slenderness calculated using the steps similar to calculating  $\lambda_l$ .

$$\lambda_{lf} = \lambda_l = \sqrt{rac{M_{
m y}}{M_{
m crl}}}$$

 $\eta$ : is determined from Fig. 15 by choosing the correspondent curve. For DM-1.5,  $\lambda_{lf}=0.43{<}0.776$  ( $\lambda_{lf}=0.43$ obtained from CUFSM [36])

Since  $\lambda_{if}$  < 0.776, therefore

$$M_{DSM-G} = \frac{\eta}{0.1565t^3 - 0.774t^2 + 1.2178t + 0.2732} \cdot \left[ M_y + \left( 1 - \frac{1}{C_{yt}^2} \right) \left( M_p - M_y \right) \right]$$

Numerical application:  $M_{crl}$ = 32035359.4 N.mm;  $M_p$  = 7599992.4 N.mm;  $M_y$ = 5943480 N.mm;  $\lambda_{lf}$  = 0.43;  $C_{yl}$  = 1.34

Here t = 1.5 mm and  $\eta = 1$ ; Therefore:

$$\begin{array}{l} \textit{M}_{DSM-G} = \frac{1}{0.1565(1.5)^3 - 0.774(1.5)^2 + 1.2178(1.5) + 0.2732} \Big[ 5943480 + \Big(1 - \frac{1}{(1.34)^2}\Big) (7599992 - 5943480) \, \Big] \\ \textit{M}_{DSM-G} = 7531663N.mm \approx 7532kN.mm \text{ (See Table 11).} \end{array}$$

(b) For specimen CV-0.48, the material properties E=216 GPa and  $\sigma_{0.2}=598$  MPa.

For CV section, we have to use Eq. 10 replicated below:

$$M_{DSM-G} = \eta. (0.1565t^3 - 0.774t^2 + 1.2178t + 0.2732) M_{nl}$$
(13)

Here  $\eta = 0.86$  and t = 0.48.

For  $M_{nl}$  calculation in case of CV-0.48 we use the same steps as adopted in the previous case. In this example we directly used the value extracted from Wang & Young (2016) [29,30], Therefore,

$$M_{DSM-G} = 0.86 \cdot \left(0.1565(0.48)^3 - 0.774(0.48)^2 + 1.2178(0.48) + 0.2732\right) \cdot 2018 = 1209kN.mm$$
 (See Table 15).

#### References

- Meza FJ, Becque J, Hajirasouliha I. Experimental study of cold-formed steel builtup beams. J Struct Eng 2020;146(7):04020126. https://doi.org/10.1061/(ASCE) ST.1943-541X.0002344.
- [2] Ye J, Meza FJ, Hajirasouliha I, Becque J, Shepherd P, Pilakoutas K. Experimental investigation of cross-sectional bending capacity of cold-formed steel channels subject to local-distortional buckling interaction. J Struct Eng 2019;145(7): 04019064. https://doi.org/10.1061/(ASCE)ST.1943-541X.00023.
- [3] Dar MA, Fayaz SJ, Rather S, Dar AR, Hajirasouliha I. Incremental stiffening approach for CFS built-up-beams with large imperfections: Tests and flexuralbehaviour. Struct 2023;53:1318–40. https://doi.org/10.1016/j. istruc.2023.05.003.
- [4] Dar MA, Anbarasu M, Dar AR, Islam NU, Ghowsi AF, Carvalho H. Stiffening schemes for CFS built-up I-beams with large global imperfections: capacity and behaviour. Steel Compos Struct 2022;42(4):447–58. https://doi.org/10.12989/ scs. 2022.43.4.447
- [5] Karthik C, Anbarasu M, Dar MA. Cold-formed ferritic stainless steel closed-section built-up beams: tests and flexural response. Thin-Walled Struct 2022;180:109820. https://doi.org/10.1016/i.tws.2022.109820.
- [6] Dar MA, Yusuf M, Dar AR, Raju J. Experimental study on innovative sections for cold formed steel beams. Steel Compos Struct 2015;19(6):1599–610. https://doi. org/10.12989/scs.2015.19.6.1599.
- [7] Dar MA, Subramanian N, Atif M, Dar AR, Anbarasu M, Lim JB. Efficient cross-sectional profiling of built up CFS beams for improved flexural performance. Steel Compos Struct 2020;34(3):333–45. https://doi.org/10.12989/scs.2020.34.3.333.
- [8] El-Taly B, El-shami M. Structural performance of cold-formed steel face-to-face and back-to-back beams. Int J Civ Eng 2021;19(12):1427–44. https://doi.org/10.1007/ act/000-021-06666.
- [9] Muftah F, Mohd Sani MS, Mohd Kamal MM. Flexural strength behaviour of bolted built-up cold-formed steel beam with outstand and extended stiffener. Int J Steel Struct 2019;19:719–32. https://doi.org/10.1007/s13296-018-0157-0.
- [10] Wang C, Guo Q, Zhang Z, Guo Y. Experimental and numerical investigation of perforated cold-formed steel built-up I-section columns with web stiffeners and complex edge stiffeners. Adv Struct Eng 2019;22(10):2205–21. https://doi.org/ 10.1177/1369433219836174.
- [11] Ye J, Hajirasouliha I, Becque J, Pilakoutas K. Development of more efficient cold-formed steel channel sections in bending. Thin-Walled Struct 2016;101:1–3. https://doi.org/10.1016/j.tws.2015.12.021.
- [12] Dubina D, Ungureanu V, Gîlia L. Experimental investigations of cold-formed steel beams of corrugated web and built-up section for flanges. Thin-Walled Struct 2015; 90:159–70. https://doi.org/10.1016/j.tws.2015.01.018.
- [13] Dar MA, Subramanian N, Dar AR, Majid M, Haseeb M, Tahoor M. Structural efficiency of various strengthening schemes for cold-formed steel beams: Effect of global imperfections. Steel Compos Struct 2019;30(4):393–403. https://doi.org/ 10.12989/scs.2019.30.4.393.
- [14] Dar AR, Anbarasu M, Arun Kumar G. Cold-formed steel built-up i-beam with the trapezoidal corrugated web: tests and numerical simulation. J Inst Eng (India): Ser A 2021;102:943–58. https://doi.org/10.1007/s40030-021-00571-8.
- [15] Wu Y, Du X, Yuan H. Structural performance of cold-formed steel box girders with C-section flanges and sinusoidal corrugated webs. Struct 2021;34:4851–66. https://doi.org/10.1016/j.istruc.2021.10.066.
- [16] Ravi D, Ponsubbiah AR, Prabha SS, Saratha JP. Experimental, analytical and numerical studies on concrete encased trapezoidally web profiled cold-formed steel

- beams by varying depth-thickness ratio. Front Struct Civ Eng 2020;14:930–46.  $\label{eq:https://doi.org/10.1007/s11709-020-0652-1}.$
- [17] Dar MA, Subramanian N, Dar AR, Anbarasu M, Lim JB, Atif M. Behaviour of partly stiffened cold-formed steel built-up beams: experimental investigation and numerical validation. Adv Struct Eng 2019;22(1):172–86. https://doi.org/ 10.1177/1369433218782267.
- [18] Dar MA, Subramanian N, Rather AI, Dar AR, Lim JB, Anbarasu M, et al. Effect of angle stiffeners on the flexural strength and stiffness of cold-formed steel beams. Steel Compos Struct 2019;33(2):225–43. https://doi.org/10.12989/ ses 2019 33 2 225
- [19] Sifan M, Gatheeshgar P, Navaratnam S, Nagaratnam B, Poologanathan K, Thamboo J, et al. Flexural behaviour and design of hollow flange cold-formed steel beam filled with lightweight normal and lightweight high strength concrete. J Build Eng 2022;48:103878. https://doi.org/10.1016/j.jobe.2021.103878.
- [20] Hegyi P, Dunai L. Experimental study on ultra-lightweight-concrete encased coldformed steel structures Part I: stability behaviour of elements subjected to bending. Thin-Walled Struct 2016;101:75–84. https://doi.org/10.1016/j.tws.2016.01.004.
- [21] Valsa Ipe T, Sharada Bai H, Manjula Vani K, Iqba MM. Flexural behavior of cold-formed steel concrete composite beams. Steel Compos Struct 2013;14(2):105–20. https://doi.org/10.12989/scs.2013.14.2.105.
- [22] Dar MA, Ghowsi AF, Dar AR, Salam SU, Anbarasu M, Vivek KS, et al. Development of lightweight CFS composite built-up beams: Tests and flexural response. J Constr Steel Res 2023;209:108041. https://doi.org/10.1016/j.jcsr.2023.108041.
- [23] Dar MA, Subramanain N, Ghowsi AF, Anbarasu M, Hajirasouliha I, Haris S, et al. Intermittently stiffened cold-formed steel GFRP composite lightweight built-up beams: experimental investigation and performance assessment. Thin-Walled Struct 2023;185:110630. https://doi.org/10.1016/j.tws.2023.110630.
- [24] Dar MA, Subramanian N, Anbarasu M, Dar AR, Lim JB. Structural performance of cold-formed steel composite beams. Steel Compos Struct 2018;27(5):545–54. https://doi.org/10.12989/scs.2018.27.5.545.
- [25] Dar MA, Subramanian N, Dar DA, Dar AR, Anbarasu M, Lim JB, et al. Flexural strength of cold-formed steel built-up composite beams with rectangular compression flanges. Steel Compos Struct 2020;34(2):171–88. https://doi.org/ 10.12989/scs.2020.34.2.171.
- [26] Anbarasu M, Dar MA, Ghowsi AF, Dar AR. Flexural behaviour of cover plated CFS built-up beams composed of lipped channels: comparison of test and design strengths. Struct 2021;30:294–304. https://doi.org/10.1016/j.istruc.2020.12.088.
- [27] Ghannam M. Bending moment capacity of cold-formed steel built-up beams. Int J Steel Struct 2019;19(2):660–71. (https://doi-org.libproxyl.nus.edu.sg/10.1007/s1 3296-018-0155-2)
- [28] Anbarasu M. Simulation of flexural behaviour and design of cold-formed steel closed built-up beams composed of two sigma sections for local buckling. Eng Struct.;191:549–562. https://doi.org/10.1016/j.engstruct.2019.04.093.
- [29] Wang L, Young B. Behavior of cold-formed steel built-up sections with intermediate stiffeners under bending. I: tests and numerical validation. J Struct Eng 2016;142 (3):04015150. https://doi.org/10.1061/(ASCE)ST.1943-541X.0001428.
- [30] Wang L, Young B. Behavior of cold-formed steel built-up sections with intermediate stiffeners under bending. II: parametric study and design. J Struct Eng 2016;142 (3):04015151. https://doi.org/10.1061/(ASCE)ST.1943-541X.000142.
- [31] Shafer BW. Review: the direct strength method of cold-formed steel member design. J Constr Steel Res 2008;64(7/8):766–78. https://doi.org/10.1016/j. icst 2008.01.022
- [32] Selvaraj S, Madhavan M. Structural design of cold-formed steel face-to-face connected built-up beams using direct strength method. J Constr Steel Res 2019; 160:613–28. https://doi.org/10.1016/j.jcsr.2019.05.053.

- [33] Glauz RS. Enhancements to the Direct Strength Method of cold-formed steel member design. Thin-Walled Struct 2023;183:110421. https://doi.org/10.1016/j. tws.2022.110421.
- [34] AISI (American Iron and Steel Institute). North American Specification for the Design of Cold-Formed Steel Structural Member. S100-16. Washington, DC: AISI; 2016.
- [35] Wang L, Young B. Behaviour and design of cold-formed steel built-up section beams with different screw arrangements. Thin-Walled Struct 2018;131:16–32. https://doi.org/10.1016/j.tws.2018.06.022.
- [36] B.W. Schafer. Constrained and unconstrained finite strip method (CUFSM). Version 5.01. accessed at \( \sqrt{www.ce.jhu.edu/bschafer/cufsm} \) on 1 May 2018.
- [37] Abbasi M, Khezri M, Rasmussen KJ, Schafer BW. Elastic buckling analysis of coldformed steel built-up sections with discrete fasteners using the compound strip
- $method.\ Thin-Walled\ Struct\ 2018;124:58-71.\ https://doi.org/10.1016/j.\ tws.2017.11.046.$
- [38] Abaqus. Version 6.14-5, ABAQUS/CAE User's Guide. Providence, RI, USA: Dassault Systèmes Simulia Corp; 2014.
- [39] Schafer BW, Pekoz T. Computational modelling of cold-formed steel: characterizing geometric imperfections and residual stresses. J Constr Steel Res 1998;47(3):193–210.
- [40] ASCE. Minimum Design Loads and Associated Criteria for Buildings and Other Structures. ASCE/SEI 7. Reston, VA: ASCE; 2016.
- [41] AS-NZS 1170–2 (2002) (English): Structural design actions Part 0: General principles, By Authority of New Zealand Structure Verification Method B1 / VM1, vol. 2, 2002